iScience

CellPress
OPEN ACCESS

Article

Role of the DUB enzyme USP7 in dendritic arborization, neuronal migration, and autistic-like behaviors in mice

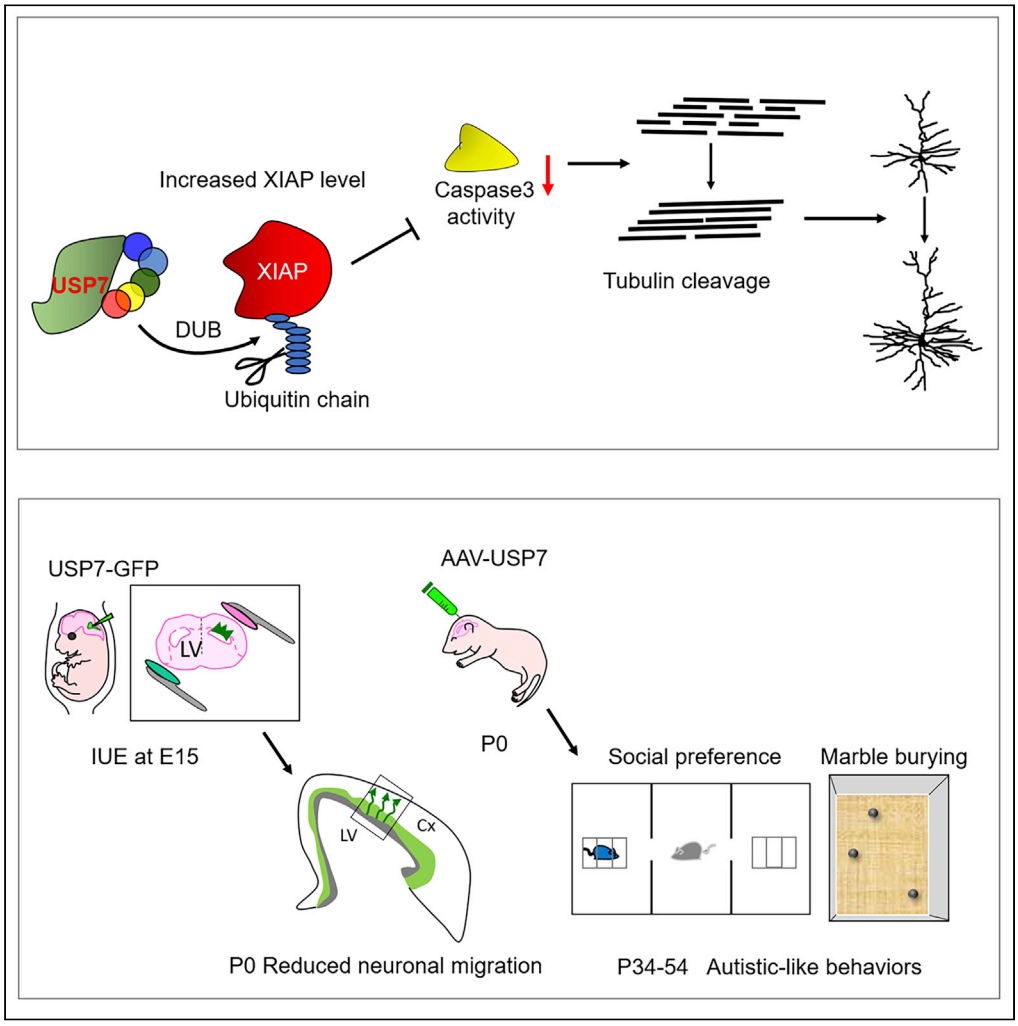

Hui Qiao, Yuan Tian, Yuda Huo, Heng-Ye Man

hman@bu.edu

Highlights

Overexpression of USP7 increases dendritic arborization

USP7 targets XIAP for deubiquitination and regulates XIAP proteostasis in neurons

USP7 regulates dendritic remodeling via the XIAP-caspase 3-tubulin pathway

Prenatal overexpression of USP7 in mice leads to autistic-like behaviors

Qiao et al., iScience 25, 104595
July 15, 2022
https://doi.org/10.1016/j.isci.2022.104595

iScience

CellPress
OPEN ACCESS

Article

Role of the DUB enzyme USP7 in dendritic arborization, neuronal migration, and autistic-like behaviors in mice

Hui Qiao,[1,2] Yuan Tian,[1] Yuda Huo,[1] and Heng-Ye Man[1,3,4,5,*]

SUMMARY

Duplication and haploinsufficiency of the USP7 gene are implicated in autism spectrum disorders (ASD), but the role for USP7 in neurodevelopment and contribution to ASD pathogenesis remain unknown. We find that in primary neurons, overexpression of USP7 increases dendritic branch number and total dendritic length, whereas knockdown leads to opposite alterations. Besides, USP7 deubiquitinates the X-linked inhibitor of apoptosis protein (XIAP). The USP7-induced increase in XIAP suppresses caspase 3 activity, leading to a reduction in tubulin cleavage and suppression of dendritic pruning. When USP7 is introduced into the brains of prenatal mice via *in utero electroporation* (IUE), it results in abnormal migration of newborn neurons and increased dendritic arborization. Importantly, intraventricular brain injection of AAV-USP7 in P0 mice leads to autistic-like phenotypes including aberrant social interactions, repetitive behaviors, as well as changes in somatosensory sensitivity. These findings provide new insights in USP7-related neurobiological functions and its implication in ASD.

INTRODUCTION

Autism spectrum disorder (ASD) appears to result from impairments throughout the multiple stages of brain development including neurogenesis, migration, neuron maturation, synaptogenesis, and synaptic communication. Protein dysregulation (Khatri et al., 2018; Kasherman et al., 2020; Han et al., 2022) and immune dysfunction (Barcellos et al., 2020; Alhosaini et al., 2021; Nadeem et al., 2021; Ahmad et al., 2021) have been suggested as the major components associated with ASD pathophysiology. Given that fine control of protein synthesis and degradation is central to the assembly of brain circuits and synaptic plasticity (Basilico et al., 2020), it is not surprising that the ubiquitin-proteasomal system (UPS) proves to be one of the core molecular hubs implicated in ASD. The UPS regulates several important neural processes that are impaired in ID/ASD, including axonal initiation, development, dendritic maturation, and synaptic maturation (Ding and Shen, 2008). Several studies have linked ASD to defects in protein degradation by identifying mutations in genes encoding UPS components including *UBE3A*, *CUL3*, *TRIP12* and USP7 (Greer et al., 2010; Martinez-Noel et al., 2012; Kasherman et al., 2020). In addition, the UPS regulates and/or integrates multiple key pathways such as WNT, mTOR and TGFβ pathways, which play important roles in brain development (Kasherman et al., 2020). Indeed, components of the UPS pathway have been considered as promising targets for therapeutic intervention in ASD (Kasherman et al., 2020).

ASDs have a strong genetic background with an increasing number of genes being discovered in the last decade (De Rubeis et al., 2014, Deciphering Developmental Disorders Study, 2015; Robinson et al., 2015; Satterstrom et al., 2020; Eyring and Geschwind, 2021). Multiple recurrent *de novo* rare copy-number variations (CNVs) are strongly associated with autism. Consistent with the key role of the UPS components in ASD, genome-wide analysis in 1124 ASD families identified rare recurrent *de novo* CNVs (duplication, 3 subjects) at 16p13.2 containing the gene ubiquitin specific protease 7 (USP7) as one of several novel ASD loci (Sanders et al., 2011). Further, another study found *de novo* heterozygous loss-of-function mutations of USP7 in 7 individuals with a neurodevelopmental disorder displaying autistic symptoms and intellectual disability (Hao et al., 2015). More recently, via genome or exome sequencing and chromosome microarray analysis, 16 individuals were reported to have heterozygous USP7 variants and demonstrated syndromes characterized by developmental delay/intellectual disability (DD/ID), autistic features of

[1]Department of Biology, Boston University, 5 Cummington Mall, Boston, MA 02215, USA

[2]College of Life Science, Shaanxi Normal University, Xi'an 710119, China

[3]Department of Pharmacology & Experimental Therapeutics, Boston University School of Medicine, 72 East Concord St., L-603, Boston, MA 02118, USA

[4]Center for Systems Neuroscience, Boston University, 610 Commonwealth Ave, Boston, MA, USA

[5]Lead contact

*Correspondence: hman@bu.edu

https://doi.org/10.1016/j.isci.2022.104595

behavioral anomalies and delays in language development (Fountain et al., 2019). These findings strongly implicate USP7 as an etiological factor in ASD.

As a DUB enzyme, USP7 acts to reverse the ubiquitination process. It is known to play an important role in cancer. It promotes the formation of regulatory T cells that block the immune response to the tumor and helps to keep p53, the primary tumor suppressor protein, at a low level, thereby allowing the tumor to grow unchecked (Bhattacharya et al., 2018). In addition, USP7 is involved in many pathways as it deubiquitinates a wide range of targets including MDM2, DNMT1, RNF168, FOXO4 and PTEN (Brooks and Gu, 2006; van der Horst et al., 2006; Song et al., 2008; Du et al., 2010; Zhu et al., 2015).

USP7 is strongly expressed in the brain, including cerebrum, cerebellum, and hippocampus (Uhlen et al., 2015). It is also expressed in the neural stem cells of the subventricular zone (SVZ) (Nicklas et al., 2019) and in hypothalamic neurons (Hao et al., 2015). However, the neural functions of USP7 are not well understood. Knockout of USP7 in mice results in early embryonic lethality, and brains from these KO mice display hypoplasia and deficiencies in brain development (Kon et al., 2011). USP7 interacts with MAGEL2, a protein implicated in Prader-Willi syndrome and ASD (Schaaf et al., 2013), as well as TRIM27 (Fountain and Schaaf, 2016). It has been hypothesized that USP7 in the brain acts as a molecular rheostat to precisely fine-tune endosomal F-actin levels by counteracting TRIM27 auto-ubiquitination and preventing overactivation of WASH (Hao et al., 2015).

To date, the neurobiological function of USP7 and the mechanistic events linking USP7 to autistic phenotypes remain unknown. We found that USP7 regulates dendritic growth via control of XIAP deubiquitination and caspase-mediated cleavage of dendritic microtubules. Overexpression of USP7 in the brain results in the dysregulation of neuron migration, dendritic arborization, and autistic-like behaviors in mice.

RESULTS

USP7 is a neuron specific protein regulating ubiquitination activities in primary neurons

USP7 is known to be expressed in the brain (Nicklas et al., 2019), but the specific cell type and brain region distribution of USP7 remain unclear. In cultured rat hippocampal neurons, we immunostained USP7 and GFAP at DIV 14. We found that USP7 was co-localized with MAP2 but not GFAP, indicating that USP7 is expressed selectively in neurons but not in glia (Figure 1A). To distinguish neuronal subtypes, we co-immunostained USP7 and a GABAergic neuronal marker GAD67. Analysis showed that USP7 expression was at the same level between excitatory and inhibitory neurons (Figure 1B). Previous studies have shown that USP7 is expressed in both the nucleus and cytoplasm of primary NSCs and neuroblasts (Nicklas et al., 2019). To determine the subcellular distribution of USP7 in neurons and its general distribution in the brain, we collected lysates of rat primary cortical neurons and tissues from multiple brain regions, and subcellular compartments were separated by centrifugation. Western blot analysis revealed that while the majority of USP7 was in the cytosol, a portion of USP7 was also distributed in the synaptosomal and nuclear compartments (Figures 1C and 1D). We then analyzed the developmental profile of USP7 expression and found that USP7 increased from E10 to P5, and then decreased drastically after P10 (Figure 1G).

Given that USP7 is a DUB enzyme (Figure S1), we wanted to determine whether USP7 is actively involved in controlling protein ubiquitination in neurons. We treated DIV15 cultured cortical neurons with HBX41108 (10 μM), a small-molecule compound that inhibits USP7 deubiquitinating activity (Colland et al., 2009), for 2 and 4 h. Western blot analysis of the cell lysates showed that the ubiquitination signals in the treated cells were significantly increased compared to the control group (HBX 2 h *vs.* Ctrl: $p < 0.01$; HBX 4 h vs. Ctrl: $p < 0.01$. $n = 4$ for each group, one-way ANOVA) (Figures 1E and 1F), indicating active DUB function of USP7 in neurons under basal conditions.

USP7 regulates neuronal dendritic growth and arborization

To investigate the role of USP7 in neuron development, we transfected primary cortical neurons with USP7 at DIV4, 7 and 11 (Figures S2A, S2B, 2A and 2E). Cells were imaged four days after transfection for structural analysis. Sholl analysis revealed a large increase in dendritic branch number and total length following USP7 overexpression from DIV 11 to DIV 15 (sholl: $F(1,44) = 13.037$, $p = 0.001$, repeated measure; No. of dendrites: $p < 0.01$; Sum length: $p < 0.01$; Ctrl: $n = 18$; USP7: $n = 22$) (Figures 2E–2H), but not in neurons expressing USP7 from DIV 4 to DIV 7 (sholl: $F(1,36) = 0.034$, $p = 0.855$, repeated measure; No. of dendrites: $p > 0.05$; Sum length: $p > 0.05$; Ctrl: $n = 18$; USP7: $n = 22$) nor from DIV 7 to DIV 11 (sholl: $F(1,56) = 3.865$,

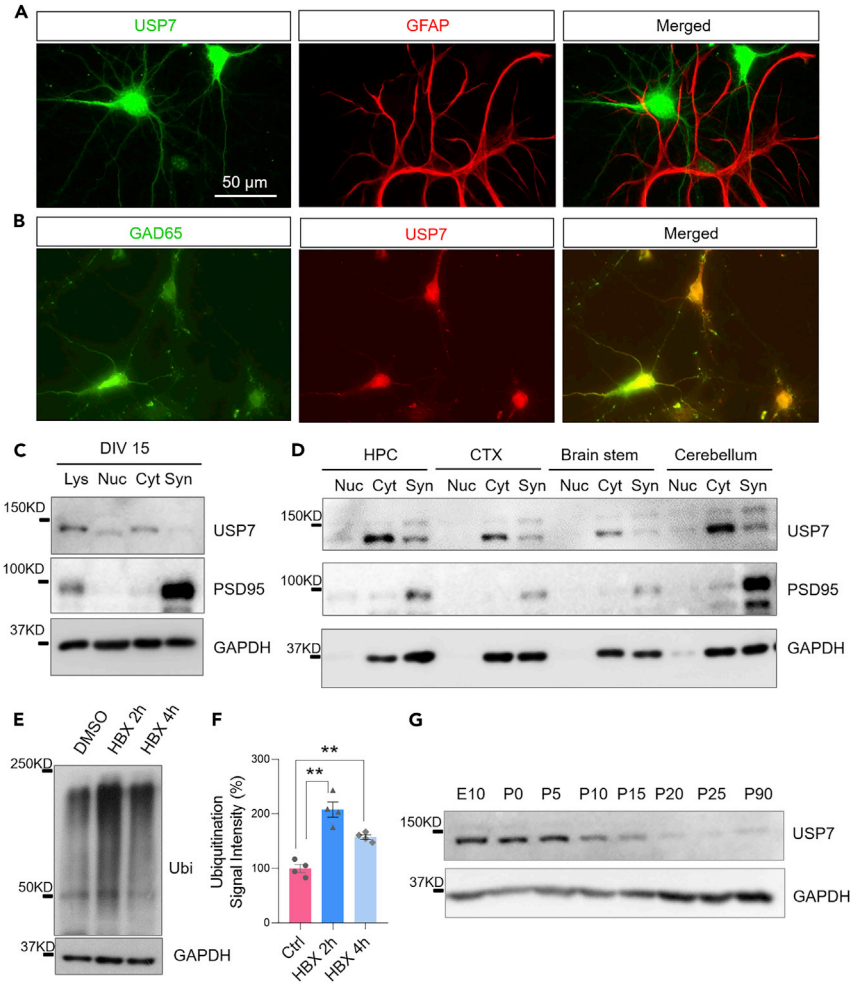

Figure 1. Expression and subcellular distribution of USP7 in neurons

(A) Immunostaining of USP7 and GFAP in rat hippocampal cultures at DIV15. Scale bar = 50 μm.

(B) Immunostaining of USP7 and GAD67 in rat hippocampal cultures at DIV15.

(C) Lysates of cultured neurons were collected on DIV15, and USP7 levels were measured by Westerns. GAPDH was probed as a loading control.

(D) Lysates of different brain regions were collected from rats of embryonic day 18. USP7 levels were measured by Western blot.

(E) Cultured neurons were treated with USP7 inhibitor HBX41108 (10 μM) for 2 or 4 h at DIV15, and the lysates were probed for ubiquitination.

(F) Quantification showed an increase in ubiquitination intensity in the HBX41108 treated group ($F(2,9) = 33.13$, $p < 0.01$, One-way ANOVA).

(G) Developmental time course of USP7 expression in the brain. Cortical tissues were collected from mice of ages from E10 to P90. Data are represented as mean ± SEM. Error bars represent SEM, **$p < 0.01$.

$p = 0.054$, repeated measure; Number of dendrites: $p > 0.05$; Sum length: $p > 0.05$; Ctrl: $n = 24$; USP7: $n = 28$) (Figures 2A–2D). These findings indicate that USP7 regulates dendrite growth at a later stage during dendritic development.

Interestingly, in the control group, we noticed that the dendrite branch number of DIV15 neurons was significantly lower than that of DIV11 cells (DIV11: 34.92 ± 1.63, $n = 24$; DIV15: 23.89 ± 2.39, $n = 18$; $p < 0.01$, *t*-test), as well as the sum length of dendrites (DIV11: 2500.99 ± 137.96, $n = 24$; DIV15: 1690.49 ± 136.79, $n = 18$; $p < 0.01$, *t*-test). In contrast, in neurons transfected with USP7, these dendritic measurements showed no difference between DIV11 and DIV15 (Number of dendrites: DIV11: 37.32 ± 1.89, $n = 28$; DIV15: 37.27 ± 3.06, $n = 22$; $p < 0.01$, *t*-test; Sum length: DIV11: 2877.19 ± 166.44, $n = 28$;

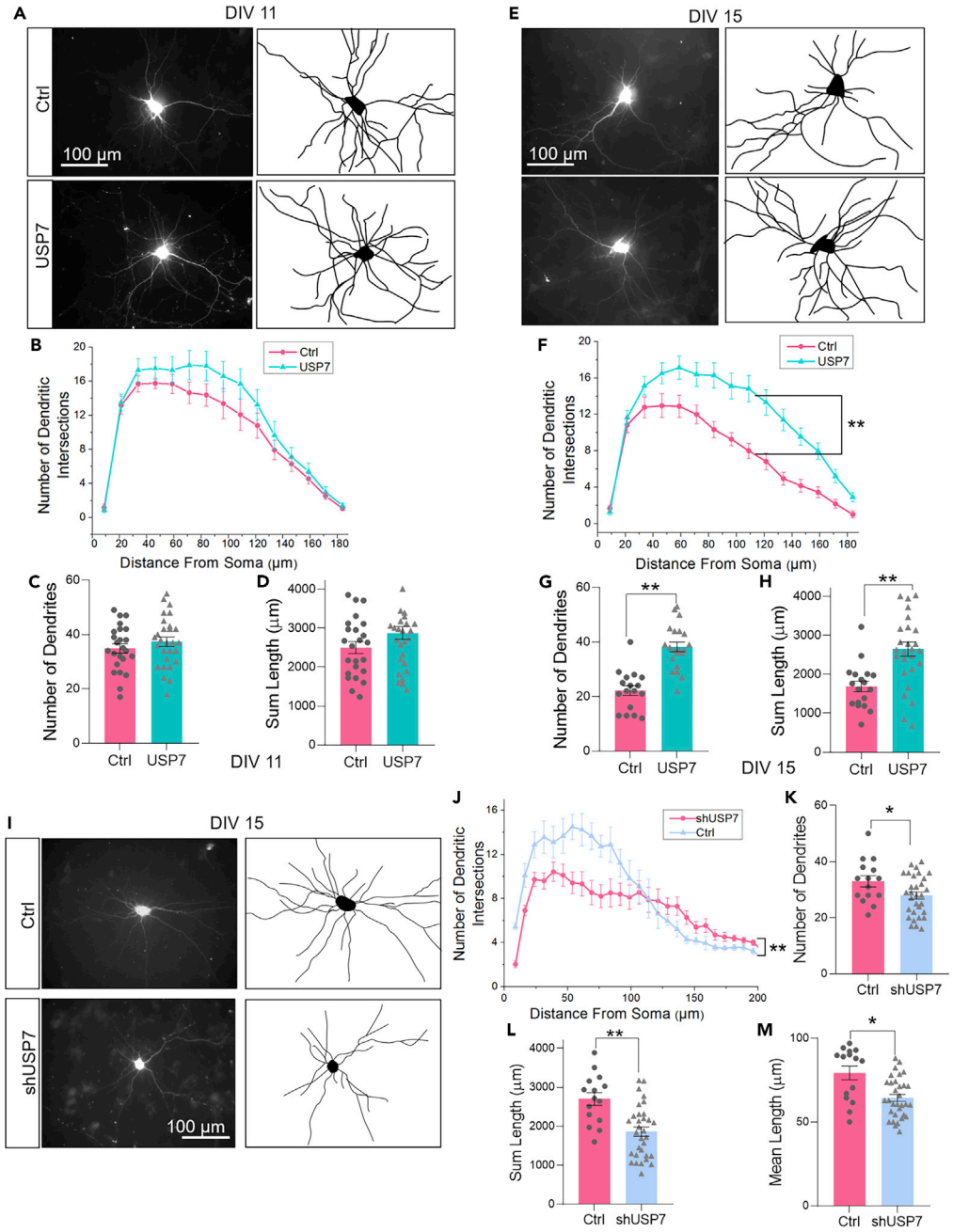

Figure 2. USP7 regulates dendritic growth and arborization

(A–D) Hippocampal neurons were transfected with a control vector or USP7 plasmid at DIV 7, and imaged for morphology at DIV 11 (A). Scale bar = 100 μm. Dendritic arborization was analyzed by Sholl analysis ($F(1,56) = 3.865$, $p = 0.054$, Repeated measures ANOVA) (B). The total number of dendritic branches and the sum length of dendrites showed no significant difference between the control (n = 24) and the USP7 group (n = 28) at DIV11 ($p > 0.05$, *t*-test) (C and D).

(E–H) Neurons were transfected with USP7 or a vector as control at DIV 11, and imaged for morphology at DIV 15 (E). Scale bar = 100 μm. Dendritic arborization was analyzed by sholl analysis ($F(1,44) = 13.037$, $p = 0.001$, Repeated measure ANOVA) (F). The total number of dendrites and total length of dendrites were increased in USP7-transfected neurons on DIV15 (Ctrl: n = 18; USP7: n = 22. Number of dendrites, $p < 0.01$, *t*-test; sum length of dendrites, $p < 0.01$, *t*-test) (G, H). Scale bar = 100 μm.

(I–M) Knockdown of USP7 results in a reduction of dendritic arborization.

(I) Cortical neurons were transfected with vector (Control, n = 16) or shUSP7 (n = 31) at DIV 11 and imaged for morphology on DIV 15. Scale bar = 100 μm.

Figure 2. *Continued*

(J) Sholl analysis of dendritic arborization at DIV 15 ($F(1,46) = 7.497$, $p = 0.009$, Repeated measure ANOVA).

(K and L) Total number of dendrites and total length of dendrites were decreased in shUSP7 neurons on DIV15 (Number of dendrites, $p < 0.05$, *t*-test; sum length of dendrites, $p < 0.01$, *t*-test).

(M) Mean length of dendrites was decreased in shUSP7 neurons on DIV15 ($p < 0.05$, *t*-test). Data are represented as mean ± SEM. Error bars represent SEM, *$p < 0.05$, **$p < 0.01$.

DIV15: 2627.01 ± 200.67, n = 22; $p > 0.05$, *t*-test) (Figures 2C, 2D, 2G and 2H). These results suggest that dendritic pruning occurred when neurons matured from DIV11 to DIV15, and USP7 overexpression blocked the pruning process, resulting in an increase in the complexity of dendritic arborization and dendritic length relative to the control neurons.

We then examined the effect of USP7 knock down on dendrite development. The effectiveness of the USP7 shRNA (shUSP7) was confirmed in transfected HEK cells (Figure 7C). Consistently, shUSP7 also caused a decrease of USP7 intensity in neurons (41.07 ± 2.13% of the control group; $p < 0.01$) (Figures S2C and S2D). We then transfected cortical neurons at DIV11 with shUSP7 and analyzed dendritic structure at DIV15. We found that knock down of USP7 suppressed dendritic arborization ($F(1,46) = 7.497$, $p = 0.009$, repeated measure) (Figures 2I and 2J). The number of dendrites (Ctrl: n = 16; shUSP7: n = 33; $p < 0.05$, *t*-test), sum dendrite length (Ctrl: n = 16; shUSP7: n = 33; $p < 0.01$, *t*-test) and mean length of dendritic branches ($p < 0.05$, *t*-test) were all markedly decreased compared with the control (Figures 2K, 2L and 2M).

USP7 expression results in an increase in XIAP protein amount in neurons

XIAP, an E3 ligase that targets caspase-3 for proteasomal degradation (Riedl et al., 2001; Suzuki et al., 2001a), inhibits the activity of the cell death proteases caspase-3, -7 and -9, and is involved in the local pruning of dendrites and spines (Erturk et al., 2014). Our previous study showed that XIAP is involved in the regulation of E6AP-dependent dendritic remodeling (Khatri et al., 2018). We therefore sought to determine whether XIAP is implicated in the effect of USP7 on dendritic development.

To examine the developmental time course of USP7 and XIAP in neurons, we collected lysates of cortical neurons at different time points from DIV 0 to DIV 20. USP7 expression increased significantly at DIV5, peaked at DIV 9, and then declined after DIV12. Interestingly, XIAP showed a similar pattern in its expression time course, with a significant increase at DIV5 and a decline after DIV12 (Figures 3A and 3B).

To explore whether USP7 targets XIAP for regulation, we infected cultured neurons with AAV-USP7 and measured XIAP expression by westerns and immunostainings. We found that the XIAP level increased significantly in neurons overexpressing USP7 compared with the control (western blot: 157.82 ± 10.31% of the control group, GFP-AAV: n = 4; USP7-AAV: n = 4, $p < 0.05$; ICC: 138.49 ± 7.24% of the control group, Ctrl: n = 13; USP7: n = 13, $p < 0.01$; *t*-test) (Figures 3C, 3D, 3E, 3H and 3I). In line with this, inhibition of USP7 activity with HBX41108 led to a decrease in XIAP accumulation ($F(2,9) = 30.88$, $p < 0.01$, One-way ANOVA, Dunnett) (Figures 3F and 3G). In addition, immunostaining also showed reduced intensities of XIAP in neurons expressing shUSP7 (64.43 ± 3.47% of the control, $p < 0.01$, *t*-test. Ctrl: n = 14; USP7: n = 14) (Figures 3J and 3K). These findings indicate a role for USP7 in the control of XIAP proteostasis.

USP7 causes XIAP deubiquitination and stabilization

We found that the XIAP protein levels were up-regulated by USP7, suggesting a role for USP7 in mediating XIAP protein turnover. To determine whether the degradation of XIAP is affected by USP7, we transfected HEK cells with FLAG-XIAP and USP7 for 48 h. Cells were then incubated with cycloheximide (CHX, 35 μM) to block protein synthesis for 0, 4, 8 h before being harvested for western blot analysis. We found that while the XIAP levels decreased over time because of degradation, the rate of decay became slower in cells co-transfected with USP7 (Treatment: $F(1,4) = 10.14$, $p < 0.05$, repeated measure) (Figures 4D and 4E), indicating that USP7 expression enhanced the stability of XIAP.

Given that USP7 is a DUB enzyme, the change in XIAP turnover by USP7 could result from changes in its ubiquitination status. To test this possibility, we transfected HEK cells with FLAG-XIAP, HA-Ubi and GFP-USP7, and performed ubiquitination assays on immunoprecipitated FLAG-XIAP from the cell lysates. Indeed, the ubiquitin signals of XIAP were significantly decreased in cells co-transfected with USP7 compared to the control ($F(2,9) = 20.95$, $p < 0.01$, one-way ANOVA, Tukey. XIAP: n = 4; XIAP + Ubi: n = 4;

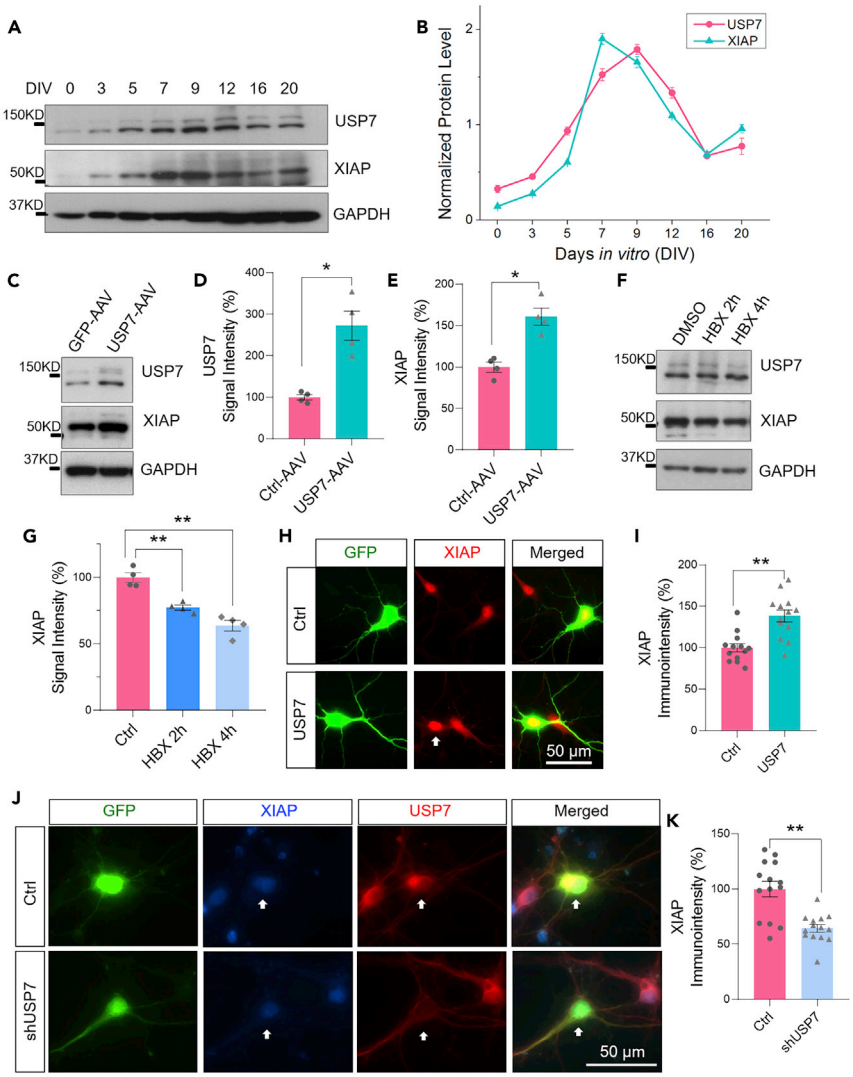

Figure 3. USP7 regulates XIAP protein accumulation in neurons

(A) Lysates were collected from primary cortical neurons of DIV 0 to DIV 20. Expression levels of USP7 and XIAP were measured by Western blot. GAPDH was probed as a loading control.

(B) Quantification of USP7 and XIAP intensity (n = 3).

(C–E) Cortical neurons were infected with AAV-GFP or AAV-USP7 on DIV 0 for 15 days, and USP7 and XIAP levels were measured by Western blot. An increased level for both USP7 and XIAP was detected in neurons infected with USP7 virus (GFP-AAV: n = 4; USP7-AAV: n = 4. $p < 0.05$, *t*-test).

(F and G) Cortical neurons were treated with HBX41108 (USP7 inhibitor) for 2 and 4 h and the lysates were collected to probe for XIAP. Inhibition of USP7 led to a decrease in XIAP amount. (Ctrl: n = 4; HBX 2 h: n = 4; HBX 4 h: n = 4. $F(2,9) = 30.88$, $p < 0.01$, one-way ANOVA, Dunnett).

(H) Cortical neurons were transfected with USP7 at DIV 11 and immunostained for XIAP at DIV 15. Scale bar = 50 μm.

(I) Quantification showed an increase in endogenous XIAP intensity in neurons transfected with USP7 (Ctrl: n = 13; USP7: n = 13. $p < 0.01$, *t*-test).

(J) Hippocampal neurons were transfected with shUSP7 at DIV 8 and immunostained for XIAP at DIV 15. Scale bar = 50 μm.

(K) Quantification showed a decrease in endogenous XIAP in neurons with USP7 knockdown (Ctrl: n = 14; USP7: n = 14. $p < 0.01$, *t*-test). Data are represented as mean ± SEM. Error bars represent SEM, *p < 0.05, **p < 0.01.

XIAP + Ubi + USP7: n = 4). Moreover, a significant decrease in XIAP was detected in cells of XIAP + Ubiquitin, but not cells also expressing USP7 ($F(2,9) = 22.20$, $p < 0.01$, one-way ANOVA, Tukey) (Figures 4A–4C), consistent with facilitated XIAP ubiquitination and degradation by ubiquitin, and deubiquitination and stabilization of XIAP by USP7.

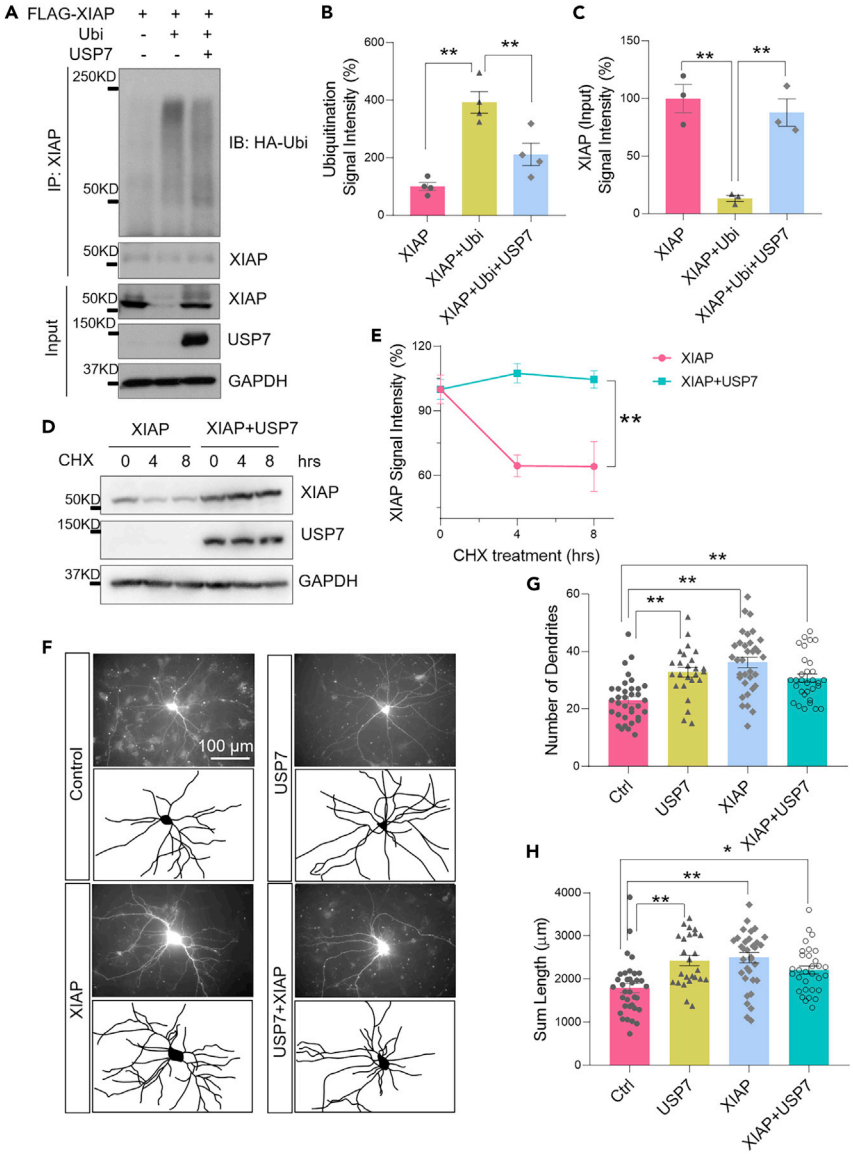

Figure 4. USP7 causes XIAP deubiquitination and stabilization

(A) XIAP ubiquitination assay. HEK293 cells were transfected with FLAG-XIAP, HA-ubiquitin, and USP7 for 2 days. XIAP was immunoprecipitated and probed for ubiquitin (ubi). Cell lysates (input) were used to detect protein levels.

(B and C) Quantification of Western blot intensities. USP7 caused a decrease in XIAP ubiquitination and a decrease in XIAP protein levels (Ubiquitination Signal: $F(2,9) = 20.95$, $p < 0.01$, one-way ANOVA, Tukey; XIAP Signal: $F(2,9) = 22.20$, $p < 0.01$, one-way ANOVA, Tukey. XIAP: n = 4; XIAP + Ubi: n = 4; XIAP + Ubi + USP7: n = 4).

(D) Degradation assay of XIAP with or without USP7. Transfected HEK cells were treated with cycloheximide (CHX) for various time periods and cell lysates were collected to examine XIAP levels by Western blot.

(E) Quantification of the degradation rate of XIAP over time (Treatment: $F(1,4) = 10.14$, $p < 0.05$, repeated measure ANOVA).

(F) Morphology of primary neurons transfected with USP7 or XIAP alone, or both. Scale bar = 100 μm.

(G and H) Dendrite branch number and the total length of dendrite were increased in neurons overexpressing USP7 or XIAP. Co-transfection of USP7 and XIAP had no additional effects compared with USP7 alone or XIAP only group (Ctrl: n = 35; USP7: n = 25; XIAP: n = 34; XIAP + USP7: n = 31. Number of dendrites: $F(3,121) = 13.83$, $p < 0.01$, one-way ANOVA, Tukey; Sum dendrite length: $F(3,121) = 8.82$, $p < 0.01$. one-way ANOVA, Tukey). Data are represented as mean ± SEM. Error bars represent SEM, *$p < 0.05$, **$p < 0.01$.

XIAP mediates the effect of USP7 on dendritic arborization

XIAP has been shown to be implicated in dendrite growth and pruning (Erturk et al., 2014; Khatri et al., 2018). Because XIAP is a substrate of USP7, we speculated that the effect of USP7 on dendritic arborization may be mediated by XIAP. To test this possibility, we transfected primary hippocampal neurons with either USP7 or XIAP alone or with both. We found that although single expression of either USP7 or XIAP led to an increase in the number of dendrites (USP7 ($n = 25$) vs. Ctrl ($n = 35$): $p < 0.01$; XIAP ($n = 34$) vs. Ctrl: $p < 0.01$. One-way ANOVA, Tukey) and total length of dendrites (USP7 vs. Ctrl: $p < 0.01$; XIAP vs. Ctrl: $p < 0.01$. One-way ANOVA, Tukey), co-expression of XIAP with USP7 showed no further increases in branching or total length of dendrites compared with either USP7 or XIAP alone (Number of dendrites: XIAP + USP7 ($n = 31$) vs. XIAP, $p = 0.06$; XIAP + USP7 vs. USP7, $p = 0.81$. One-way ANOVA, Tukey) (Sum length: XIAP + USP7 vs. XIAP, $p = 0.24$; XIAP + USP7 vs. USP7, $p = 0.54$. One-way ANOVA, Tukey) (Figures 4F–4H). These findings indicate that the effect on dendritic growth was saturated by either USP7 or XIAP, supporting the two molecules functioning along the same pathway.

We then transfected neurons with shXIAP alone or shXIAP plus USP7. Expression of shXIAP decreased the expression of XIAP (Ctrl ($n = 36$) vs. shXIAP ($n = 36$), $p < 0.01$, t-test) (Figures 5A and 5B) and suppressed dendritic arborization (sholl: Ctrl ($n = 46$) vs. shXIAP ($n = 46$), $p < 0.01$. Repeated measures ANOVA, Tukey) (Figures 5C and 5F). The number of dendrites ($p < 0.05$, one-way ANOVA, Tukey) and summed dendrite length ($p < 0.05$, one-way ANOVA, Tukey) were significantly decreased compared with the control (Figures 5D and 5E). When USP7 was co-transfected with shXIAP, we found that while USP7 alone increased dendritic complexity (sholl: Ctrl vs. USP7 ($n = 30$), $p < 0.05$, Repeated measures ANOVA, Tukey), knock down of XIAP blocked the effect of USP7 on dendritic arborization (sholl: USP7 vs. USP7+shXIAP ($n = 36$), $p < 0.01$, Repeated measures ANOVA, Tukey) and showed no difference compared with the shXIAP only group (sholl: shXIAP vs. USP7+shXIAP, $p < 0.01$, Repeated measures ANOVA, Tukey) (Figures 5C and 5F). The summed length and total number of dendrites showed a comparable reduction between shXIAP and the shXIAP + USP7 groups (Sum length: shXIAP ($n = 46$) vs. USP7+shXIAP ($n = 35$), $p > 0.05$; Number of dendrites: shXIAP ($n = 46$) vs. USP7+shXIAP ($n = 35$), $p > 0.05$. one-way ANOVA, Tukey) (Figures 5C–5E). This result indicates that up-regulation of XIAP is necessary for the regulatory effect of USP7 on dendrites.

In our previous study, we demonstrated that the E3 ligase Ube3A/E6AP catalyzes ubiquitination of XIAP, leading to XIAP degradation and dendritic pruning (Khatri et al., 2018). To investigate whether E6AP and USP7 have antagonizing effects on XIAP ubiquitination, HEK293T cells were transfected with HA-ubiquitin, FLAG-XIAP, together with E6AP, or E6AP and USP7. Two days after transfection, XIAP was isolated by immunoprecipitation and probed for HA-ubiquitin signals. Consistent with our previous study (Khatri et al., 2018), we found that E6AP overexpression markedly enhanced XIAP ubiquitination (XIAP + Ubi + E6AP ($n = 4$) vs. XIAP + Ubi ($n = 4$), $p < 0.05$, Tukey). In contrast, XIAP ubiquitination levels were significantly reduced in cells expressing both E6AP and USP7 (XIAP + Ubi + E6AP + USP7 ($n = 4$) vs. XIAP + Ubi + E6AP, $p < 0.01$, Tukey), indicating that USP7 competes with E6AP to balance the status of XIAP ubiquitination (Figures 6A–6C).

To examine whether the antagonizing effect of E6AP and USP7 at XIAP ubiquitination and protein stability is related to dendritic arborization, we co-transfected E6AP together with USP7 in cultured neurons at DIV 11. Sholl analysis at DIV 15 showed that E6AP expression caused a significant reduction in dendritic complexity and length (sholl analysis: Group: $F(3,77) = 16.833$, $p < 0.01$. E6AP ($n = 19$) vs Ctrl ($n = 20$): $p < 0.01$, Repeated measures ANOVA, Tukey), but the E6AP-induced down-regulation in dendritic growth was abolished by co-expression with USP7 (USP7+E6AP ($n = 21$) vs E6AP: $p < 0.01$; Repeated measures ANOVA, Tukey) (Figures 6D–6G). (Number of dendrites: $F(3,81) = 17.28$, $p < 0.01$. one-way ANOVA, Tukey; Sum dendrite length $F(3,81) = 17.92$, $p < 0.01$. one-way ANOVA, Tukey).

The XIAP-caspase3 pathway is involved in the effect of USP7 on dendritic arborization

In the caspase cascade, the activated caspases function via proteocleavage of effector target proteins, which results in a wide-range of cellular functions (Erturk et al., 2014; Khatri et al., 2018). In neurons, caspase activity plays an important role in dendritic and spine regulation (Jiao and Li, 2011; Erturk et al., 2014). Because XIAP inhibits the cleavage and activation of caspase3 by acting as a brake on caspase3-mediated downstream cellular events (Huang et al., 2004), we sought to investigate whether USP7 can regulate the activity of the caspase cascade via XIAP. In line with this, we found that in HEK cells, overexpressing USP7 resulted in a significant decrease, whereas knockdown of USP7 caused an increase in cleaved activated caspase3. ($F(2,6) = 16.56$, $p < 0.01$, One-way ANOVA, Tukey) (Figures 7C and 7D). Similarly, in cultured neurons,

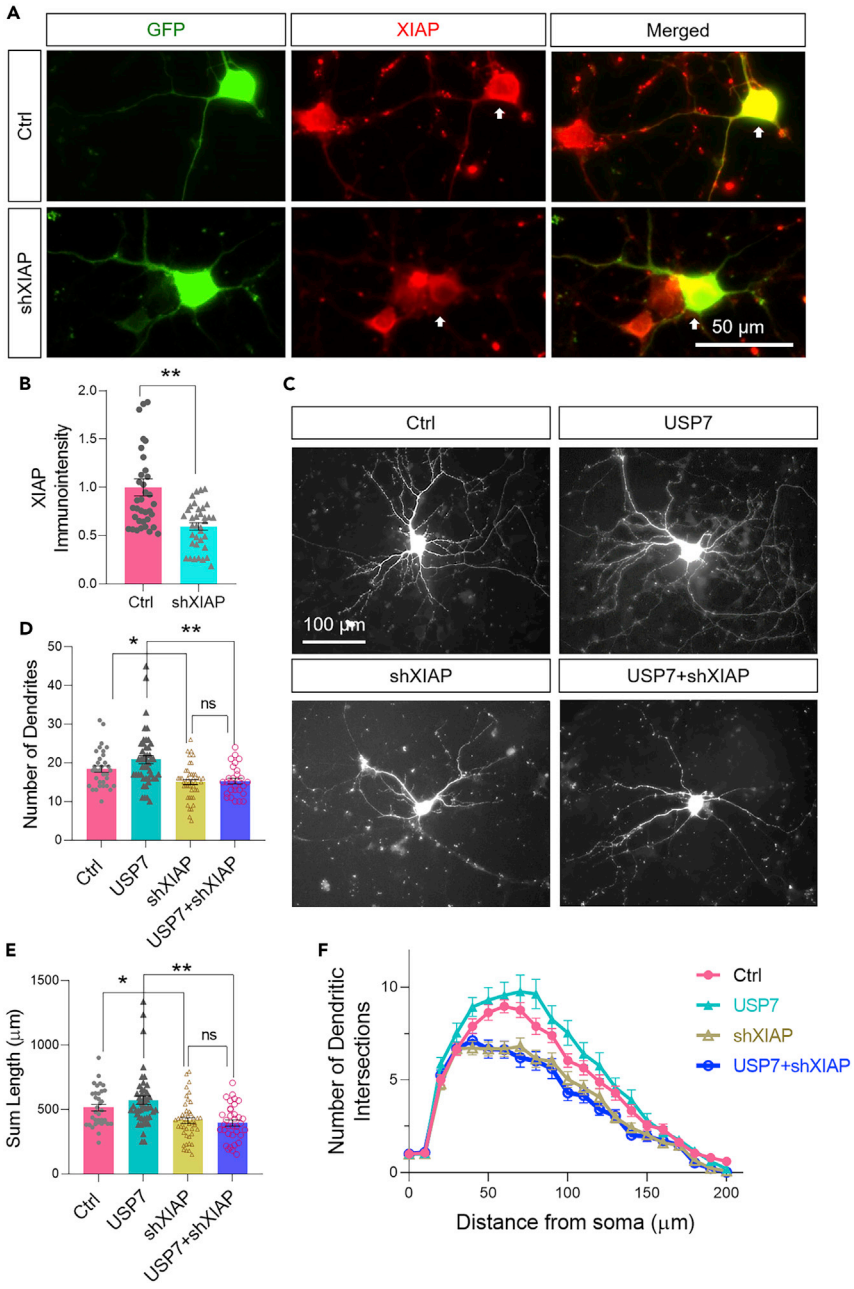

Figure 5. Knockdown of XIAP blocks the effect of USP7 on dendritic arborization

(A) Cultured neurons were transfected with shXIAP at DIV 7 and immunostained for XIAP at DIV 11. Scale bar = 50 μm.

(B) Quantification of XIAP expression (Ctrl: n = 36; shXIAP: n = 36. $p < 0.01$, *t*-test).

(C) Morphology of primary neurons transfected with USP7 or shXIAP alone, or both at DIV11. Scale bar = 100 μm.

(D and E) Dendrite branch number and the total length of dendrite were decreased in XIAP knockdown neurons. Co-transfection of USP7 and shXIAP had no additional effects compared with shXIAP alone group, but decreased significantly compared with USP7 only group (Ctrl: n = 35; USP7: n = 46; shXIAP: n = 46; USP7+shXIAP: n = 35. Number of dendrites: $F(3,148) = 10.69$, $p < 0.01$, one-way ANOVA, Tukey; Sum dendrite length: $F(3,148) = 10.01$, $p < 0.01$. one-way ANOVA, Tukey).

(F) Sholl analysis of dendritic arborization at DIV 11 (Group: $F(3, 154) = 11.23$, $p < 0.01$. Ctrl vs. shXIAP: $p < 0.01$; Ctrl vs. USP7: $p > 0.05$; USP7+shXIAP vs. USP7: $p < 0.01$; USP7+shXIAP vs. shXIAP: $p > 0.05$. Repeated measures ANOVA, Tukey). Data are represented as mean ± SEM. Error bars represent SEM, *$p < 0.05$, **$p < 0.01$.

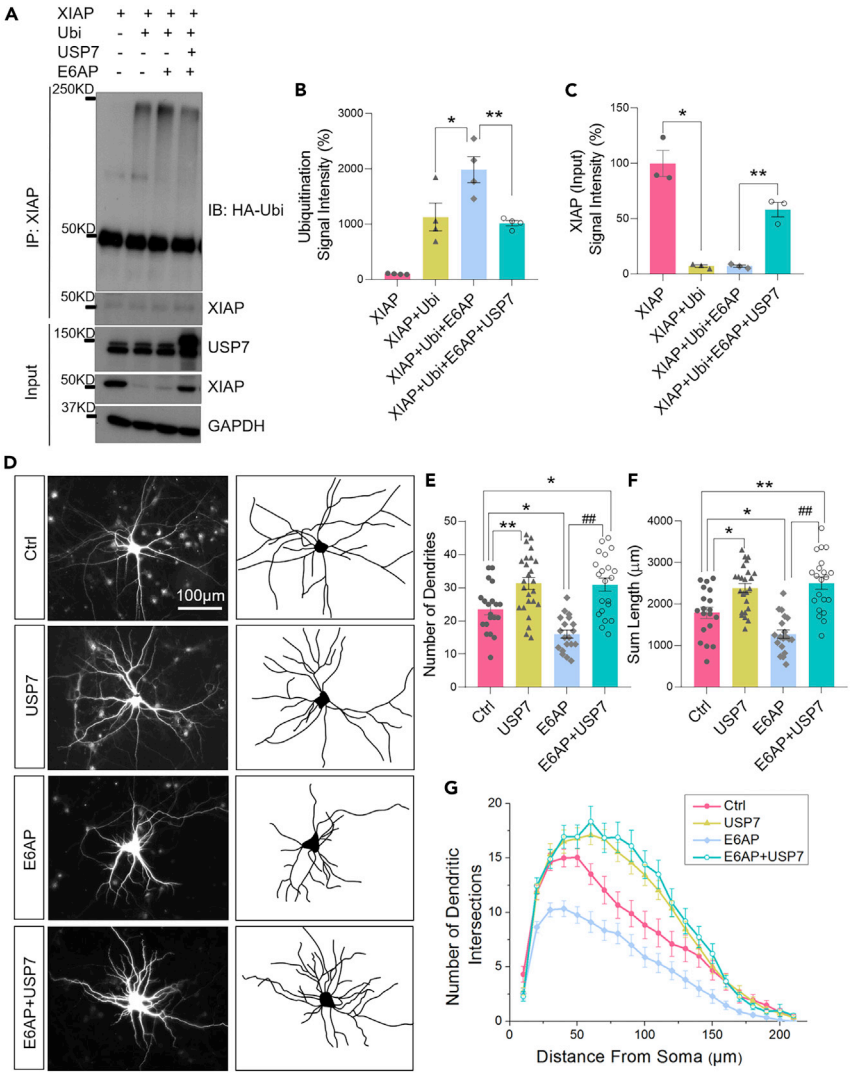

Figure 6. USP7 antagonizes E6AP effect on dendritic arborization via control of XIAP ubiquitination

(A) HEK293 cells were transfected with FLAG-XIAP, HA-ubiquitin, and USP7 with or without E6AP for 2 d. XIAP was immunoprecipitated and probed for HA-ubiquitin (HA-ubi). Cell lysates (input) were also probed to detect the total protein levels.

(B and C) Quantification of western blot intensities. E6AP caused an increase in XIAP ubiquitination ($F(3,12) = 19.62$, $p < 0.01$, one-way ANOVA, Tukey) and a decrease in XIAP protein levels in the input ($F(3,8) = 43.69$, $p < 0.01$, one-way ANOVA, Tukey). USP7 blocked the effect of E6AP on XIAP protein accumulation and XIAP ubiquitination.

(D) Morphology of primary neurons transfected with USP7, E6AP, and USP7+E6AP (DIV 11 - DIV 15). Scale bar = 100 μm.

(E and F) Dendritic branch number ($F(3,81) = 17.28$, $p < 0.01$, one-way ANOVA, Tukey) and the total length of dendrites ($F(3,81) = 17.92$, $p < 0.01$, one-way ANOVA, Tukey) were decreased in neurons with E6AP overexpression (E6AP: n = 19; Ctrl: n = 20. one-way ANOVA, Tukey). USP7 abolished the effect caused by E6AP expression (E6AP + USP7: n = 21; E6AP: n = 19. one-way ANOVA, Tukey).

(G) Sholl analysis showed a reduction in the complexity of dendritic arborization in E6AP neurons, which was blocked by co-expression with USP7 in neurons (Group: $F(3,77) = 16.833$, $p < 0.01$. Repeated measures ANOVA, Tukey). Data are represented as mean ± SEM. Error bars represent SEM, *$p < 0.05$, **$p < 0.01$.

overexpression of USP7 also decreased the intensity of cleaved caspase3 (Ctrl (n = 15) vs. USP7 (n = 19), $p < 0.01$, *t*-test) (Figures 7A and 7B).

Studies have shown that in cells including neurons, tubulin is an important substrate of caspase3 and is cleaved by activated caspase3 (Sokolowski et al., 2014). Given that microtubules are the core supportive

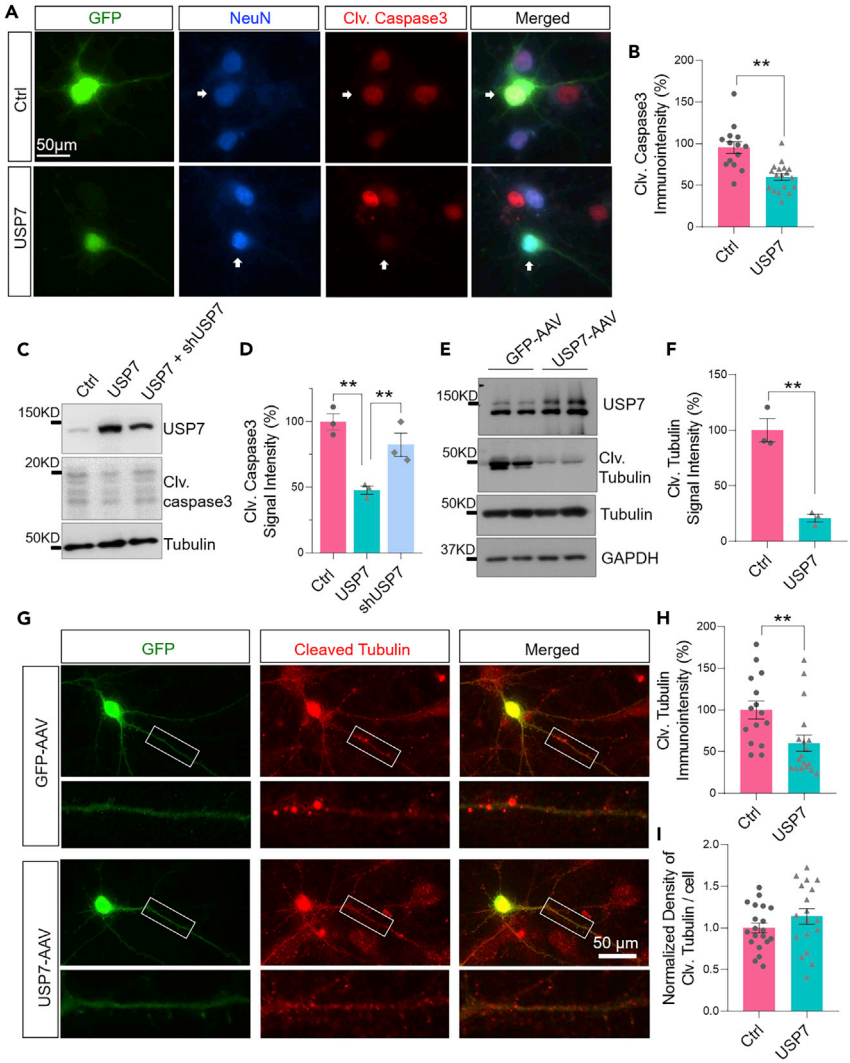

Figure 7. Caspase-3 and microtubules are the downstream effectors mediating the USP7 effect on dendritic arborization

(A) Primary hippocampal neurons were transfected with USP7 and immunostained for the cleaved caspase 3. Arrows indicate the transfected neurons. Scale bar = 50 μm.

(B) Quantification showed a decrease in cleaved caspase-3 intensity in USP7 overexpressing neurons (Ctrl: n = 15; USP7: n = 19, *t*-test).

(C) HEK cells were transfected with USP7 and shUSP7. Cell lysates were collected to determine the cleaved caspase-3 levels by Westerns.

(D) Quantification of Western blot intensities of cleaved caspase-3 ($F(2,6) = 16.56$, $p < 0.01$, one-way ANOVA, Tukey).

(E) Primary neurons were infected with AAV-USP7 at DIV 0, and neuron lysates were collected for western blot to detect changes in microtubule cleavage.

(F) Quantification showed a significant decrease in cleaved microtubules in neurons with USP7 virus infection (Ctrl: n = 3; USP7: n = 3, *t*-test).

(G) Primary neurons were infected with AAV-USP7 at DIV 0 and immunostained at DIV 15 with TubΔCasp6 antibodies. Scale bar = 50 μm.

(H and I) Quantification showed that USP7-infected neurons had a decrease in microtubule cleavage intensity (Ctrl: n = 15; USP7: n = 18, *t*-test), but not in the number of cleavage sites along the dendrite (Ctrl: n = 20; USP7: n = 18, *t*-test). Data are represented as mean ± SEM. Error bars represent SEM, *$p < 0.05$, **$p < 0.01$.

structures in dendrites, it is conceivable that microtubule destruction by the caspase cascade should lead to dendritic destabilization and structural reorganization. Indeed, the cleavage of tubulin by caspase3 and caspase6 has been shown to be involved in cytoskeletal degradation during axon degeneration (Sokolowski et al., 2014) and in dendritic remodeling (Erturk et al., 2014; Khatri et al., 2018). We therefore speculated whether tubulin cleavage plays a role in the effects of USP7 on dendritic arborization. By immunostaining with the antibody TubΔCasp6 against tubulin cleavage sites (Klaiman et al., 2008; Sokolowski et al., 2014), we found that the intensity of tubulin cleavage signals was decreased significantly in USP7-infected neurons (Ctrl (n = 15) vs. USP7(n = 18), $p < 0.01$, *t*-test) (Figures 7G–7I). To further characterize this cleavage, cell lysates were collected at DIV15, and western blot results revealed a significant reduction in cleaved tubulin compared to the control (Ctrl (n = 3) vs. USP7(n = 3), $p < 0.01$, *t*-test) (Figures 7E and 7F).

In vivo expression of USP7 in the brain causes dysregulation in neuron migration and dendritic development

As we found that USP7 was highly expressed from E10 to P10 in the brain, the time window critical for neuron migration, cortical layer formation, and also the early stage of dendrite outgrowth and spine development (Gilbert and Man, 2017; Farhy-Tselnicker and Allen, 2018), it is intriguing to explore the role for USP7 in brain development. We overexpressed USP7 in the prenatal mouse brain by *in utero electroporation* (IUE) during early development (Figure 8A). The USP7-GFP plasmids or a control GFP vector was electroporated in the mouse brain at E15, and at P0, the affected brains were prepared for immunostaining to determine the effect of USP7 overexpression. When neuronal migration was analyzed, we found that at P0, 81.75% of control neurons had already reached the upper CP. In contrast, for neurons with USP7 overexpression, only 55.49% reached this region (Figures 8B and 8C). In line with this, 11.41 and 2.41% of GFP control neurons were found in the lower CP and VZ, while 17.87 and 19.46% of USP7 electroporated neurons were distributed in these two regions, respectively (Figures 8B and 8C). These results indicate that neuron migration was suppressed by USP7 overexpression.

We then examined the effects of USP7 on neuron morphological maturation. At P15, sholl analysis revealed a significant increase in dendritic arborization in neurons electroporated with USP7 ($F(1, 48) = 17.06$, $p < 0.01$) (Figures 8D and 8E). The number of dendrites (Ctrl (n = 27) vs. USP7 (n = 22), $p < 0.01$, *t*-test) and the total length of dendrites (Ctrl (n = 27) vs. USP7 (n = 22), $p < 0.01$, *t*-test) were both increased in neurons overexpressing USP7 at layer III and layer V (Figures 8F and 8G). Consistent with our findings in primary neurons *in vitro*, these results show that overexpression of USP7 *in vivo* in the brain results in alterations in neuronal development, including migration and dendritic arborization.

Viral expression of USP7 in mouse brain leads to autistic-like behaviors and changes in pain sensitivity

Given that dosage changes of USP7, including duplication and haploinsufficiency, are implicated in ASD (Sanders et al., 2011; Fountain et al., 2019) and other neurodevelopmental phenotypes (e.g. Schaaff-Yang syndrome; Duan et al., 2021), we wanted to evaluate the effect of USP7 overexpression on brain function and behaviors. To this end, we performed bilateral intracerebroventricular injections of AAV GFP-USP7 or AAV GFP as control (2 μL each side) in mouse brains at P0. Animals were later subjected to different behavioral tests at P30 to P55 (Figure 9A).

To first confirm virus expression, brain tissues and brain slices were prepared from mice following virus injection at P0. The expression of GFP-USP7 or GFP control was detected in the entire brain from P30 to P60. In the cortex, stronger expression was observed in layer III and layer V (Figures 9B and 9C). Western blots showed that USP7 expression in the cortex was significantly higher in AAV USP7 groups than in the controls. Consistently, the level of XIAP was also increased in the brains injected with USP7 virus (Figure 9D). We then evaluated neuron morphological development (Figures 9E–9I). Sholl analysis of layer V cortical neurons in the somatosensory cortex revealed that neurons infected with USP7 virus had a more complex dendritic arborization compared to the control group (Group: $F(1, 44) = 37.91$, $p < 0.01$, Repeated measures ANOVA, 19 cortical neurons from 4 control mice and 27 cortical neurons from 5 AAV USP7 mice). The number of dendrites, and the mean and total length of dendrites, were significantly increased in the AAV USP7 group (Number of dendrites: Ctrl (n = 19) vs. USP7 (n = 27), $p < 0.01$; Sum length: Ctrl vs. USP7: $p < 0.01$; Mean length: Ctrl vs. USP7: $p < 0.01$. *t*-test). These *in vivo* changes by USP7 are consistent with our findings in primary neurons *in vitro*.

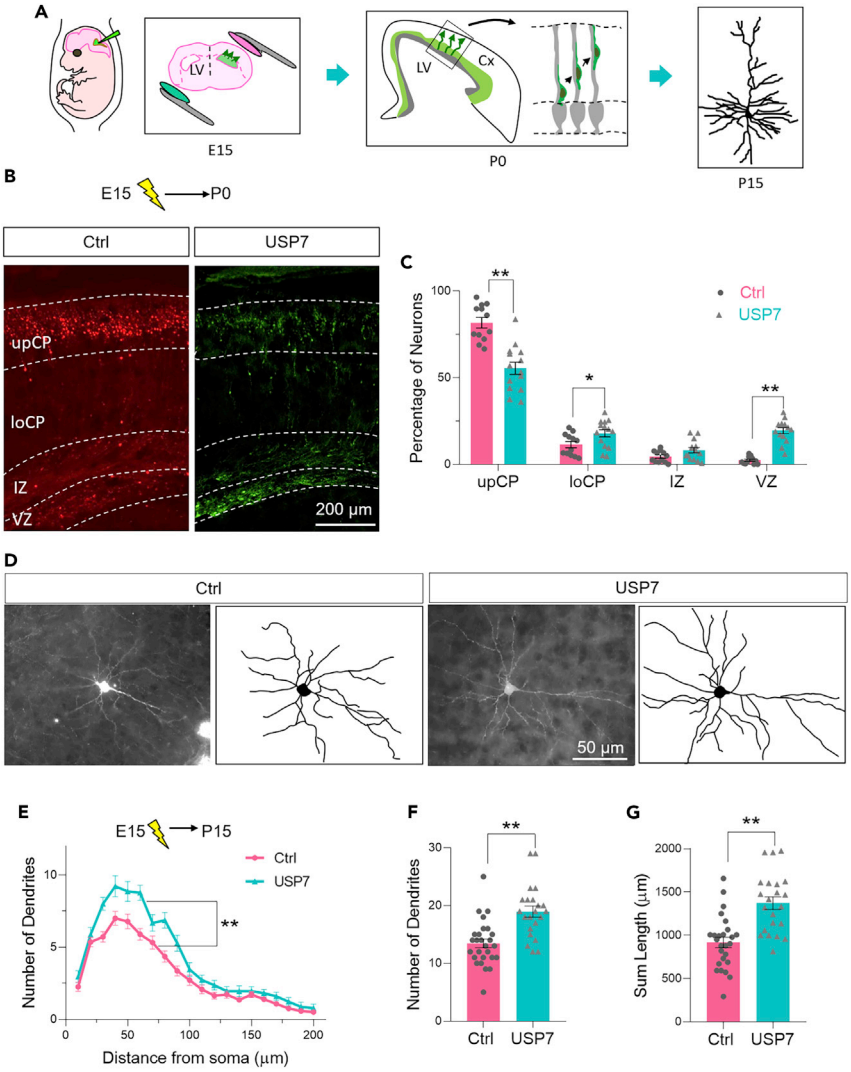

Figure 8. USP7 overexpression in the brain affects neuron migration and dendritic arborization

(A) Schematic illustration of the procedures for *in utero electroporation* (IUE) performed at E15 and P0, P15.

(B) Brain slices taken at P0 following IUE of DsRed control (Ctrl) or GFP-USP7 at E15. Scale bar = 200 μm.

(C) Analysis of neuronal migration at P0 showed that less neurons were distributed in the upCP and more in the loCP and VZ regions compared with controls (Ctrl: n = 12; USP7: n = 14. *t*-test). More than 1200 GFP^+ neurons from four brains were analyzed in each group. 15 slices from five brains were analyzed in each group, and more than 3000 GFP^+ neurons were analyzed totally.

(D) Representative images showing dendritic arborizations of control and USP7 groups. Scale bar = 50 μm.

(E) Sholl analysis of dendritic structure at P15 after IUE showed a significant change in branching (Group: $F(1, 48) = 17.06$, $p < 0.01$, Repeated measures ANOVA. Ctrl: n = 27; USP7: n = 22).

(F and G) Dendrite numbers and the total length of dendrites were increased in the USP7 overexpressing group compared with the control (Ctrl: n = 27; USP7: n = 22. *t*-test). Data are represented as mean ± SEM. Error bars represent SEM, *$p < 0.05$, **$p < 0.01$.

If viral expression of USP7 in the brain altered signaling events and neuronal development, we wanted to determine whether it also led to abnormalities in brain function and behavior. We first examined animal activities at the home cage. We found that mice injected with USP7 virus showed increased activities in grooming (Ctrl (n = 9) vs. USP7 (n = 11), $p < 0.05$, *t*-test) and digging (Ctrl (n = 8) vs. USP7 (n = 12), $p < 0.05$, *t*-test) compared with the control (Figure 10A). The overall activity level, assessed by the total number of activities including grooming, rearing, digging, climbing, circling and jumping, was also increased significantly in the AAV USP7 group compared with the AAV GFP control (Ctrl (n = 8) vs. USP7 (n = 11),

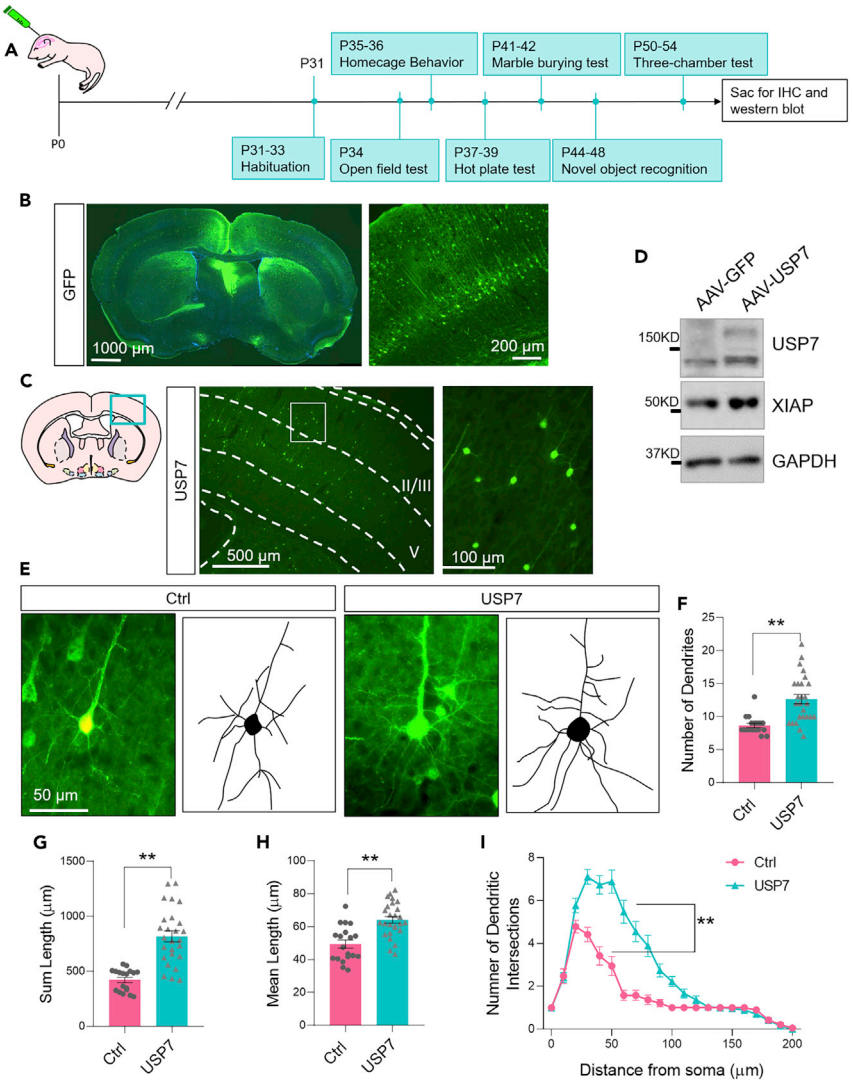

Figure 9. USP7 overexpression *in vivo* in mouse brain at P0 leads to dendrite morphological changes

(A) Schematic illustration of the procedures for virus injection at P0 and schedule for behavior tests performed at P30-P55. AAV-USP7 and AAV-GFP were injected into the lateral ventricles in mice at P0, and the mice were perfused around P30 to P60 for cryostat to show the validity of the virus. The expression of GFP (B) or GFP-fused USP7 (left: Scale bar = 1000 μm; right: Scale bar = 200 μm) (C) can be detected in the whole brain around P30 to P60 (left: Scale bar = 500 μm; right: Scale bar = 100 μm).

(D) Western blot showed that the expression of USP7 in the cortex of the AAV USP7 group is significantly higher than in the control group, as well as XIAP.

(E–I) Sholl analysis shows the morphological changes. Scale bar = 50 μm. 19 cortical neurons from 5 control mice and 27 neurons from 5 AAV USP7 mice were analyzed. The number of dendrites and the mean and total length of dendrites were all increased significantly in the AAV USP7 group (F, Number of dendrites: Ctrl: n = 19, USP7: n = 27, $p < 0.01$, *t*-test; G,Sum length: Ctrl: n = 19, USP7: n = 27, $p < 0.01$, *t*-test; H, Mean length: Ctrl: n = 19, USP7: n = 27, $p < 0.01$. *t*-test). I, The dendritic arborization was more complex in the AAV USP7 group compared with the control group (Group: $F(1, 44) = 37.91$, $p < 0.01$, Repeated measures ANOVA). Data are represented as mean ± SEM. Error bars represent SEM, *$p < 0.05$, **$p < 0.01$.

$p < 0.05$, *t*-test) (Figure 10B). However, in the open field test, the track length showed no difference between the two groups (Ctrl (n = 9) vs. USP7 (n = 13), $p > 0.05$, *t*-test) (Figure 10C). In marble burying test (Figure 10D), the AAV USP7 mice buried significantly more marbles than the control mice during a 30 min episode (Ctrl (n = 9) vs. USP7 (n = 13), $p < 0.05$, *t*-test) (Figures 10D–10F).

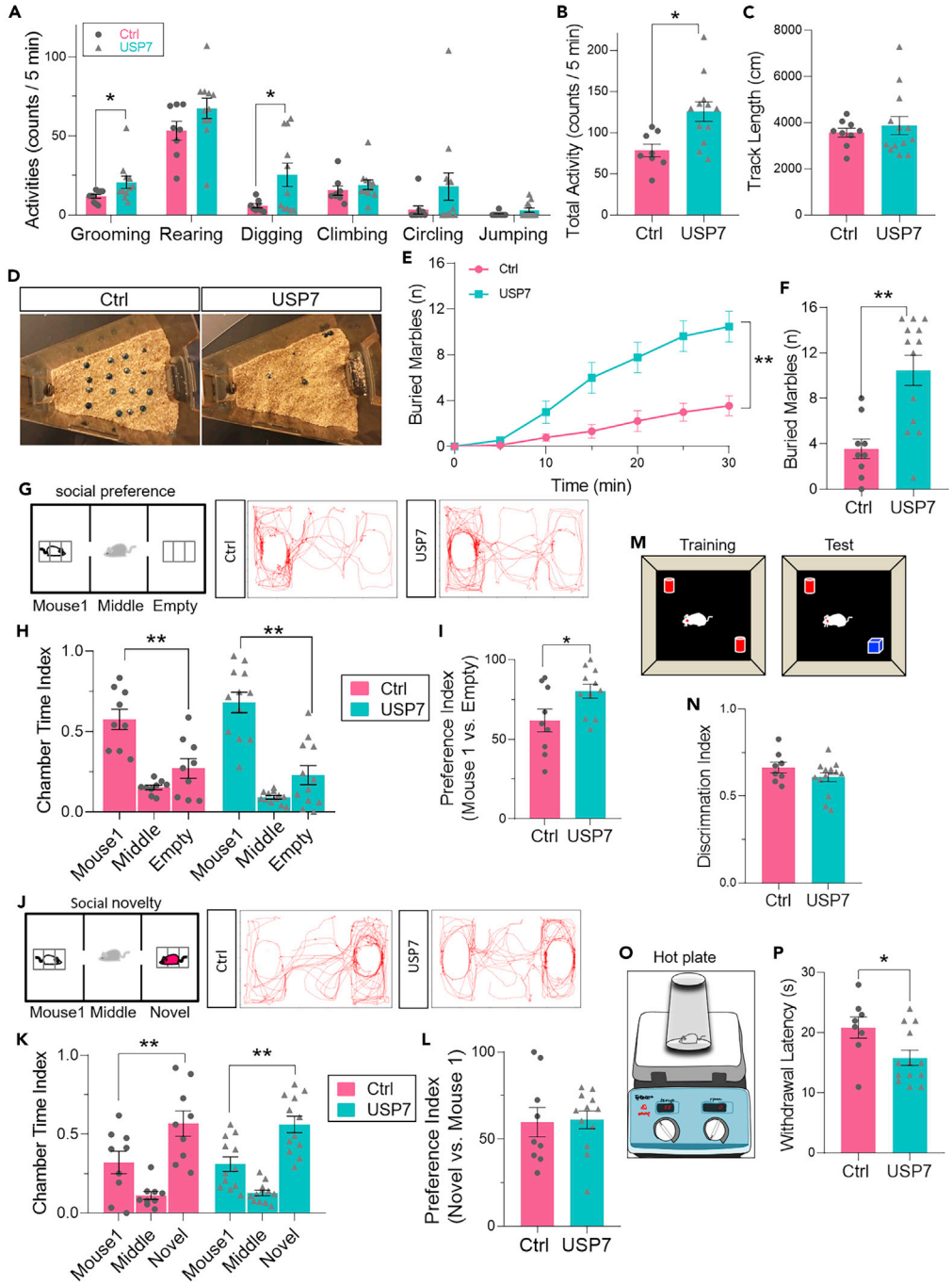

Figure 10. Behavior changes in mice following USP7 overexpression in the brain at P0. Behavioral tests were performed at P30-P55

(A and B) Homecage activities including grooming, rearing, digging, climbing, circling, and jumping (Ctrl: n = 9; USP7: n = 13, *t*-test). Counts of grooming and digging (A), as well as the overall activity events (B), were increased significantly in USP7 infected mice.

(C) Track length in the open field test showed no difference between two groups (*t*-test).

(D) A representative example of the test arena at the end of the Marble burying test.

(E) USP7 mice buried more marbles during the test ($F(1,20) = 13.46$, $p < 0.01$. Ctrl: n = 9; USP7: n = 13, repeated measures ANOVA).

(F) Quantification of the number of marbles buried at the end of the test (30 min).

(G and J) Paradigm for the social preference test (G) and social novelty test (J), and representative tracing.

Figure 10. *Continued*

(H and K) Quantification of time spent in each chamber in the social preference test (H) (Ctrl: n = 8; USP7: n = 12, *t*-test) and social novelty test (K) (Ctrl: n = 8; USP7: n = 12, *t*-test).

(I and L) Quantification of the preference index in the social preference test (I) and social novelty test (L). The preference for social interaction was increased in USP7 animals compared with the control (*t*-test) (I).

(M and N) The novel object recognition test showed no difference in discrimination index between the two groups (Ctrl: n = 8; USP7: n = 13, *t*-test).

(O and P) Hot plate test. The withdrawal latency was decreased in USP7 mice compared with the control (Ctrl: n = 8; USP7: n = 13, *t*-test). Data are represented as mean ± SEM. Error bars represent SEM, *p < 0.05, **p < 0.01.

Defect in social behaviors is one of the hallmarks in ASD (Moretti et al., 2005; Feyder et al., 2010; Vogt et al., 2015; Gilbert and Man, 2017). We thus sought to determine changes in the social behaviors in mice with USP7 overexpression. In the three-chamber sociability test, a stranger mouse was placed into one side chamber, while the other side chamber was left empty (Figure 10G). We found that while both the USP7 mice and the control mice spent a significantly longer time in the stranger-containing chamber than the empty chamber (Figure 10H), USP7 mice showed a higher score in the preference index (Figure 10I) (Ctrl (n = 9) vs. USP7 (n = 11), $p < 0.05$, *t*-test). We then placed a novel mouse into the empty chamber to test social novelty (Figure 10J), and no difference in preference index was detected between the USP7 mice and control mice (Figures 10K and 10L) (Ctrl (n = 9) vs. USP7 (n = 12), $p > 0.05$, *t*-test), indicating a minimal role of USP7 overexpression on social novelty behaviors. We then examined cognitive function by assessing novel object recognition (Figure 10M). Two identical objects were introduced to the mouse, and 24 h later, one of the familiarized objects was replaced with a novel object. Data analysis showed that both the control mice and the USP7 mice spent more time interacting with the novel object, and no difference was detected in the discrimination index between the two groups (Figure 10N) (Ctrl (n = 8) vs. USP7 (n = 13), $p > 0.05$, *t*-test), indicating intact recognition capabilities in mice with USP7 overexpression. In addition, in ASD patients and model animals, alterations were often found in the peripheral somatosensory functions (Sukoff Rizzo and Crawley, 2017; Kurokawa et al., 2021). We performed the hot plate assay to evaluate thermal sensitivity in virus-injected mice by measuring the latency of hindpaw withdrawal (Figure 10O). The USP7 mice showed a shorter withdrawal latency than the control mice (Figure 10P) (Ctrl (n = 8) vs. USP7 (n = 13), $p < 0.05$, *t*-test), indicating an up-regulation in thermal pain sensitivity because of USP7 overexpression in the brain.

DISCUSSION

In this study, we investigated the neurobiological function of USP7 and its implication in the ASD phenotype. Our findings reveal an important role for USP7 in the regulation of dendrite growth and structural maturation. Overexpression of USP7 resulted in an increase, whereas knockdown of USP7 led to a decrease in dendrite branching and length. Interestingly, we found that the dendritic arborization was reduced on DIV15 relative to DIV 11. However, this reduction in dendritic arborization was abolished by USP7 overexpression. Therefore, the positive regulatory effect on dendritic growth by USP7 is likely achieved via disrupting the developmental structural remodeling of the dendrites by suppression of the dendritic pruning process. Consistent with our *in vitro* results, expression of USP7 *in vivo* in mouse brain by IUE at E15 led to an increase in dendrite branch number and dendrite total length when examined at P15. In addition, USP7 overexpression also resulted in a change in neuronal redistribution in cortical layers. Newborn neurons overexpressing USP7 were distributed more at the inner cortical region as compared to control neurons, indicating an inhibitory effect of USP7 in neuron migration.

XIAP is the most potent member of the IAP gene family in its ability to suppress caspase activity and apoptosis (Suzuki et al., 2001b; Abbas and Larisch, 2020). XIAP is implicated in axon degeneration, as it has been shown that sustaining XIAP levels in degenerating axons reduces caspase activation and suppresses axonal degeneration (Unsain et al., 2013). Our previous study demonstrated that XIAP is involved in Ube3A/E6AP-induced dendritic remodeling (Khatri et al., 2018).

XIAP is known to be a target of ubiquitination (Tse et al., 2011) and can be stabilized by proteasome inhibition (Galban and Duckett, 2010). In fact, XIAP has intrinsic ligase activity and can ubiquitinate itself. RING domains can function as E3 ligases by binding to E2 ubiquitin-conjugating enzymes (UBCs) and recruiting E2s to a substrate. XIAP, as well as another RING-containing IAP, is capable of autoubiquitination in a manner dependent on its RING (Yang et al., 2000; Vaux and Silke, 2005; Galban and Duckett, 2010). It is likely that the intrinsic biological activity of XIAP is also controlled by transubiquitination. ARTS associates

with XIAP and causes XIAP ubiquitination and degradation by interacting with the E3 ligase Siah-1 (seven in absentia homolog 1) (Garrison et al., 2011; Abbas and Larisch, 2020). It has been shown that XIAP phosphorylation protects XIAP from ubiquitination and degradation (Dan et al., 2016). Another study demonstrated that USP9X deubiquitylates and stabilizes XIAP in mitosis (Engel et al., 2016). Our results show that the expression level of XIAP matches that of USP7, with both reaching a high expression level before DIV12, and then decreasing. Using AAV USP7 and USP7 inhibitor treatments, we observed corresponding changes in both USP7 and XIAP. The degradation and ubiquitination assays confirmed that USP7 up-regulates the stability of XIAP via deubiquitination. Importantly, we found that XIAP plays a key role in mediating the effect of USP7 in dendrite development. Mimicking the effect of USP7, XIAP overexpression also increased the branch number and summed dendritic length, whereas knockdown of XIAP blocked the effect of USP7. In line with these findings, co-expression of USP7 with XIAP did not have an additive effect relative to either alone, indicating that XIAP acts as an effector downstream of USP7. Also, our previous study demonstrated that E6AP suppresses dendritic growth via a downregulation of XIAP (Khatri et al., 2018), suggesting a molecular process opposite to that underlying USP7 effect. In support of this idea, our results revealed that USP7 overexpression was able to block E6AP-induced XIAP ubiquitination and dendritic retraction. Thus, the turnover and amount of XIAP are regulated by the abundance of USP7.

To further investigate the effect of USP7 overexpression at an early developmental age on behavioral performance, we delivered AAV USP7 into the lateral ventricle of mice at P0 and conducted behavior tests at their adolescent ages (P30-P55). Elevated levels in self-grooming and marble burying behaviors are typical autistic-like behaviors in mice (Nadeem et al., 2019, 2020; Al-Mazroua et al., 2019). Indeed, apparent repetitive behaviors, such as grooming, digging, circling, and jumping, were observed in the USP7 mice. Mice injected with USP7 virus showed increased marble burying activities, increased preference to social stimuli in the three-chamber test, and increased sensitivity to pain stimuli, but no changes were detected in the memory tests.

Elevated grooming and marble burying activities are common autistic behaviors observed in transgenic mice with ASD risk genes. In addition, although no significant difference in locomotor activity in the open field test was observed, mice overexpressing USP7 showed an increase in overall activity events including grooming, jumping, digging and others, which could suggest a phenotype of hyperactivity. Stereotyped jumping, circling or digging may also be considered as repetitive behaviors (Sukoff Rizzo and Crawley, 2017; Lee et al., 2018). Clinical studies estimate that the prevalence of co-occurring ASD and hyperactivity or attention deficits in children ranges from 20% to 50% (Levy et al., 2010; McClain et al., 2017). Many ASD animal models, such as *Ptchd1* KO mice (Murakami et al., 2019), mice with a deletion mutation in the CBP CH1 domain (CBPΔCH1/ΔCH1) (Zheng et al., 2016), *Cntnap2* KO, Neuroligin-3 KO and shank2 KO mice also show hyperactivity phenotypes (Radyushkin et al., 2009; Penagarikano et al., 2011; Schmeisser et al., 2012; Kazdoba et al., 2016).

Interestingly, in the behavior tests, we found that mice overexpressing USP7 showed elevated sociability. Indeed, though ASDs are typically associated with reduced social activities, the opposite trait of hypersociability and indiscriminate friendliness can also occur in individuals with specific neurodevelopmental disorders, such as Williams syndrome, Angelman syndrome and 17q21.31 microdeletion syndrome (Koolen-De Vries syndrome) (Stoppel and Anderson, 2017; Toth, 2019). Deletion of chromosome 15q11-q13 (including *UBE3A*) in Angelman syndrome causes developmental delay and a typical behavioral profile including a happy demeanor and increased motor behavior (Bower and Jeavons, 1967). In line with this, mice lacking the maternally inherited *Ube3a* gene ($Ube3a^{mKO}$) show an increased social preference and a longer social interaction time in the three-chamber social test (Stoppel and Anderson, 2017). Hypersociability in Williams syndrome is accompanied by a poor understanding of social dynamics, facial expression, and body language (Dykens, 2003; Toth, 2019). Studies indicate that reduced amygdala responses to fearful facial expressions may underlie social disinhibition, whereas an increased amygdala response to happy facial expressions could explain the high motivation of Williams patients to interact with others (Haas et al., 2009, 2010; Toth, 2019). It is thus intriguing to study the role of USP7 in specific brain regions and circuits involved in social behaviors.

Limitations of the study

Intraventricular virus injection was performed in P0 mice; therefore, the contribution of USP7 effect on prenatal brain development to autistic behaviors was not evaluated in this study. In addition, the virus expression may not be affecting the entire brain to a similar extent, and the viral USP7 protein level at brain regions may not mimic the physiological pattern of USP7 expression. Transgenic mice of USP7 gene duplication will be a better paradigm to study the autistic traits.

STAR★METHODS

Detailed methods are provided in the online version of this paper and include the following:

- KEY RESOURCES TABLE
- RESOURCE AVAILABILITY
  - Lead contact
  - Materials availability
  - Data and code availability
- EXPERIMENTAL MODEL AND SUBJECT DETAILS
- METHOD DETAILS
  - Neuronal and cell line transfection
  - Viral constructs preparation and virus infection
  - Biochemical analysis of protein ubiquitination
  - Western blot
  - *In utero* electroporation
  - Intraventricular brain injection of adeno-associated virus (AAV2) in neonatal mice
  - Behavioral tests
  - Open field test
  - Homecage behavior test
  - Hot plate test
  - Marble burying test
  - Novel object recognition (NOR) test
  - Three-chamber test
  - Immunohistochemistry of brain slices
- QUANTIFICATION AND STATISTICAL ANALYSIS
  - Experimental design and statistical analyses
  - Sholl analysis

SUPPLEMENTAL INFORMATION

Supplemental information can be found online at https://doi.org/10.1016/j.isci.2022.104595.

ACKNOWLEDGMENTS

We thank members of the Man Laboratory for helpful discussions and comments on this study and thank Kathrynann Odamah for assistance in manuscript preparation. We thank Dr. Andrea LeBlanc (McGill University) for providing the antibody for cleaved tubulin TubΔCasp6. This work was supported by the National Institutes of Health (R01 MH079407).

AUTHOR CONTRIBUTIONS

H.Y.M. designed the experiments and supervised the study. H.Q. designed and conducted the experiments, and analyzed most of the data. Y.T. analyzed the behavioral data. Y.H. conducted the IUE experiments. H.Y.M. and H.Q. prepared the figures and the manuscript. All authors approve of the final version of the manuscript.

DECLARATION OF INTERESTS

The authors declare no competing interests.

INCLUSION AND DIVERSITY

We worked to ensure sex balance in the selection of non-human subjects.

Received: October 14, 2021
Revised: March 15, 2022
Accepted: June 8, 2022
Published: July 15, 2022

REFERENCES

Abbas, R., and Larisch, S. (2020). Targeting XIAP for promoting cancer cell death-the story of ARTS and SMAC. Cells *9*. https://doi.org/10.3390/cells9030663.

Ahmad, S.F., Bakheet, S.A., Ansari, M.A., Nadeem, A., Alobaidi, A.F., Attia, S.M., Alhamed, A.S., Aldossari, A.A., and Mahmoud, M.A. (2021). Methylmercury chloride exposure aggravates proinflammatory mediators and Notch-1 signaling in CD14(+) and CD40(+) cells and is associated with imbalance of neuroimmune function in BTBR T(+) Itpr3tf/J mice. Neurotoxicology *82*, 9–17. https://doi.org/10.1016/j.neuro.2020.10.014.

Alhosaini, K., Ansari, M.A., Nadeem, A., Bakheet, S.A., Attia, S.M., Alhazzani, K., Albekairi, T.H., Al-Mazroua, H.A., Mahmood, H.M., and Ahmad, S.F. (2021). 5-Aminoisoquinolinone, a PARP-1 inhibitor, ameliorates immune abnormalities through upregulation of anti-inflammatory and downregulation of inflammatory parameters in T cells of BTBR mouse model of autism. Brain Sci. *11*, 249. https://doi.org/10.3390/brainsci11020249.

Al-Mazroua, H.A., Alomar, H.A., Ahmad, S.F., Attia, M.S.A., Nadeem, A., Bakheet, S.A., Alsaad, A.M.S., Alotaibi, M.R., and Attia, S.M. (2019). Assessment of DNA repair efficiency in the inbred BTBR T(+)tf/J autism spectrum disorder mouse model exposed to gamma rays and treated with JNJ7777120. Prog. Neuropsychopharmacol. Biol. Psychiatry *93*, 189–196. https://doi.org/10.1016/j.pnpbp.2019.04.003.

Barcellos, H.H. d. A., Pompermaier, A., Mendonça-Soares, S., Maffi, V.C., Fernandes, M., Koakoski, G., Kirsten, K., Baldisserotto, B., and Barcellos, L.J.G. (2020). Aripiprazole prevents stress-induced anxiety and social impairment, but impairs antipredatory behavior in zebrafish. Pharmacol. Biochem. Behav. *189*, 172841. https://doi.org/10.1016/j.pbb.2019.172841.

Basilico, B., Morandell, J., and Novarino, G. (2020). Molecular mechanisms for targeted ASD treatments. Curr. Opin. Genet. Dev. *65*, 126–137. https://doi.org/10.1016/j.gde.2020.06.004.

Bhattacharya, S., Chakraborty, D., Basu, M., and Ghosh, M.K. (2018). Emerging insights into HAUSP (USP7) in physiology, cancer and other diseases. Signal Transduct. Target. Ther. *3*, 17. https://doi.org/10.1038/s41392-018-0012-y.

Bower, B.D., and Jeavons, P.M. (1967). The "happy puppet" syndrome. Arch. Dis. Child. *42*, 298–302.

Brooks, C.L., and Gu, W. (2006). p53 ubiquitination: Mdm2 and beyond. Mol. Cell *21*, 307–315.

Colland, F., Formstecher, E., Jacq, X., Reverdy, C., Planquette, C., Conrath, S., Trouplin, V., Bianchi, J., Aushev, V.N., Camonis, J., et al. (2009). Small-molecule inhibitor of USP7/HAUSP ubiquitin protease stabilizes and activates p53 in cells. Mol. Cancer Ther. *8*, 2286–2295.

Dan, H.C., Sun, M., Kaneko, S., Feldman, R.I., Nicosia, S.V., Wang, H.G., Tsang, B.K., and Cheng, J.Q. (2016). Akt phosphorylation and stabilization of X-linked inhibitor of apoptosis protein (XIAP). J. Biol. Chem. *291*, 22846. https://doi.org/10.1074/jbc.a116.312044.

De Rubeis, Silvia, He, Xin, Goldberg, Arthur P., Poultney, Christopher S., Samocha, Kaitlin, Cicek, A. Erucment, et al. (2014). Synaptic, transcriptional and chromatin genes disrupted in autism. Nature *515* (6526), 209–215. https://doi.org/10.1038/nature13772.

Deciphering Developmental Disorders Study (2015). Large-scale discovery of novel genetic causes of developmental disorders. Nature *519*, 223–228.

Ding, M., and Shen, K. (2008). The role of the ubiquitin proteasome system in synapse remodeling and neurodegenerative diseases. Bioessays *30*, 1075–1083.

Du, Z., Song, J., Wang, Y., Zhao, Y., Guda, K., Yang, S., Kao, H.Y., Xu, Y., Willis, J., Markowitz, S.D., et al. (2010). DNMT1 stability is regulated by proteins coordinating deubiquitination and acetylation-driven ubiquitination. Sci. Signal. *3*, ra80. https://doi.org/10.1126/scisignal.2001462.

Duan, Y., Liu, L., Zhang, X., Jiang, X., Xu, J., and Guan, Q. (2021). Phenotypic spectrum and mechanism analysis of Schaff Yang syndrome: a case report on new mutation of MAGEL2 gene. Medicine (Baltimore) *100*, e26309. https://doi.org/10.1097/md.0000000000026309.

Dykens, E.M. (2003). Anxiety, fears, and phobias in persons with Williams syndrome. Dev. Neuropsychol. *23*, 291–316.

Engel, K., Rudelius, M., Slawska, J., Jacobs, L., Ahangarian Abhari, B., Altmann, B., Kurutz, J., Rathakrishnan, A., Fernandez-Saiz, V., Brunner, A., et al. (2016). USP9X stabilizes XIAP to regulate mitotic cell death and chemoresistance in aggressive B-cell lymphoma. EMBO Mol. Med. *8*, 851–862.

Ertürk, A., Wang, Y., and Sheng, M. (2014). Local pruning of dendrites and spines by caspase-3-dependent and proteasome-limited mechanisms. J. Neurosci. *34*, 1672–1688.

Eyring, K.W., and Geschwind, D.H. (2021). Three decades of ASD genetics: building a foundation for neurobiological understanding and treatment. Hum. Mol. Genet. R236–R244. https://doi.org/10.1093/hmg/ddab176.

Farhy-Tselnicker, I., and Allen, N.J. (2018). Astrocytes, neurons, synapses: a tripartite view on cortical circuit development. Neural Dev. *13*, 7. https://doi.org/10.1186/s13064-018-0104-y.

Feyder, M., Karlsson, R.M., Mathur, P., Lyman, M., Bock, R., Momenan, R., Munasinghe, J., Scattoni, M.L., Ihne, J., Camp, M., et al. (2010). Association of mouse Dlg4 (PSD-95) gene deletion and human DLG4 gene variation with phenotypes relevant to autism spectrum disorders and Williams' syndrome. Am. J. Psychiatry *167*, 1508–1517.

Fountain, M.D., and Schaaf, C.P. (2016). Prader-willi syndrome and schaaf-yang syndrome: neurodevelopmental diseases intersecting at the MAGEL2 gene. Diseases *4*. https://doi.org/10.3390/diseases4010002.

Fountain, M.D., Oleson, D.S., Rech, M.E., Segebrecht, L., Hunter, J.V., McCarthy, J.M., Lupo, P.J., Holtgrewe, M., Moran, R., Rosenfeld, J.A., et al. (2019). Pathogenic variants in USP7 cause a neurodevelopmental disorder with speech delays, altered behavior, and neurologic anomalies. Genet. Med. 1797–1807. https://doi.org/10.1038/s41436-019-0433-1.

Galbán, S., and Duckett, C.S. (2010). XIAP as a ubiquitin ligase in cellular signaling. Cell Death Differ. *17*, 54–60.

Garrison, J.B., Correa, R.G., Gerlic, M., Yip, K.W., Krieg, A., Tamble, C.M., Shi, R., Welsh, K., Duggineni, S., Huang, Z., et al. (2011). ARTS and Siah collaborate in a pathway for XIAP degradation. Mol. Cell *41*, 107–116.

Gilbert, J., and Man, H.Y. (2016). The X-linked autism protein KIAA2022/KIDLIA regulates neurite outgrowth via N-Cadherin and delta-Catenin signaling. eNeuro *3*. https://doi.org/10.1523/eneuro.0238-16.2016.

Gilbert, J., and Man, H.Y. (2017). Fundamental elements in autism: from neurogenesis and neurite growth to synaptic plasticity. Front. Cell. Neurosci. *11*, 359. https://doi.org/10.3389/fncel.2017.00359.

Gilbert, J., O'Connor, M., Templet, S., Moghaddam, M., Di Via Ioschpe, A., Sinclair, A., Zhu, L.Q., Xu, W., and Man, H.Y. (2020). NEXMIF/KIDLIA knock-out mouse demonstrates autism-like behaviors, memory deficits, and impairments in synapse formation and function. J. Neurosci. *40*, 237–254.

Greer, P.L., Hanayama, R., Bloodgood, B.L., Mardinly, A.R., Lipton, D.M., Flavell, S.W., Kim, T.K., Griffith, E.C., Waldon, Z., Maehr, R., et al. (2010). The Angelman Syndrome protein Ube3A regulates synapse development by ubiquitinating arc. Cell *140*, 704–716.

Haas, B.W., Hoeft, F., Searcy, Y.M., Mills, D., Bellugi, U., and Reiss, A. (2010). Individual differences in social behavior predict amygdala response to fearful facial expressions in Williams syndrome. Neuropsychologia *48*, 1283–1288.

Haas, B.W., Mills, D., Yam, A., Hoeft, F., Bellugi, U., and Reiss, A. (2009). Genetic influences on sociability: heightened amygdala reactivity and event-related responses to positive social stimuli in Williams syndrome. J. Neurosci. *29*, 1132–1139.

Han, S.T., Kim, A.C., Garcia, K., Schimmenti, L.A., Macnamara, E., Network, U.D., Gahl, W.A., Malicdan, M.C., and Tifft, C.J. (2022). PUS7 deficiency in human patients causes profound neurodevelopmental phenotype by dysregulating protein translation. Mol. Genet. Metab. *135*, 221–229.

Hao, Y.H., Fountain, M.D., Jr., Fon Tacer, K., Xia, F., Bi, W., Kang, S.H.L., Patel, A., Rosenfeld, J.A., Le Caignec, C., Isidor, B., et al. (2015). USP7 acts as a molecular rheostat to promote WASH-dependent endosomal protein recycling and is mutated in a human neurodevelopmental disorder. Mol. Cell *59*, 956–969.

Huang, Y., Lu, M., and Wu, H. (2004). Antagonizing XIAP-mediated caspase-3 inhibition. Achilles' heel of cancers? Cancer Cell *5*, 1–2. https://doi.org/10.1016/s1535-6108(03)00340-4.

Huo, Y., Khatri, N., Hou, Q., Gilbert, J., Wang, G., and Man, H.Y. (2015). The deubiquitinating enzyme USP46 regulates AMPA receptor ubiquitination and trafficking. J. Neurochem. *134*, 1067–1080.

Jiao, S., and Li, Z. (2011). Nonapoptotic function of BAD and BAX in long-term depression of synaptic transmission. Neuron *70*, 758–772.

Kasherman, M.A., Premarathne, S., Burne, T.H.J., Wood, S.A., and Piper, M. (2020). The ubiquitin system: a regulatory hub for intellectual disability and autism spectrum disorder. Mol. Neurobiol. *57*, 2179–2193.

Kazdoba, T.M., Leach, P.T., and Crawley, J.N. (2016). Behavioral phenotypes of genetic mouse models of autism. Genes Brain Behav. *15*, 7–26.

Khatri, N., Gilbert, J.P., Huo, Y., Sharaflari, R., Nee, M., Qiao, H., and Man, H.Y. (2018). The autism protein Ube3A/E6AP remodels neuronal dendritic arborization via caspase-dependent microtubule destabilization. J. Neurosci. *38*, 363–378.

Klaiman, G., Petzke, T.L., Hammond, J., and Leblanc, A.C. (2008). Targets of caspase-6 activity in human neurons and Alzheimer disease. Mol. Cell. Proteomics *7*, 1541–1555.

Kon, N., Zhong, J., Kobayashi, Y., Li, M., Szabolcs, M., Ludwig, T., Canoll, P.D., and Gu, W. (2011). Roles of HAUSP-mediated p53 regulation in central nervous system development. Cell Death Differ. *18*, 1366–1375.

Kurokawa, S., Nomura, K., Miyaho, K., Sanada, K., Iwamoto, C., Naraoka, M., Yoneda, S., Tomizawa, Y., Sawae, Y., Iwanaga, R., et al. (2021). Gastrointestinal symptoms and sensory abnormalities associated with behavioral problems in children with neurodevelopmental disorders. Autism Res. 1996–2001. https://doi.org/10.1002/aur.2549.

Lee, B., Lee, K., Panda, S., Gonzales-Rojas, R., Chong, A., Bugay, V., Park, H.M., Brenner, R., Murthy, N., and Lee, H.Y. (2018). Nanoparticle delivery of CRISPR into the brain rescues a mouse model of fragile X syndrome from exaggerated repetitive behaviours. Nat. Biomed. Eng. *2*, 497–507.

Leger, M., Quiedeville, A., Bouet, V., Haelewyn, B., Boulouard, M., Schumann-Bard, P., and Freret, T. (2013). Object recognition test in mice. Nat. Protoc. *8*, 2531–2537.

Levy, S.E., Giarelli, E., Lee, L.C., Schieve, L.A., Kirby, R.S., Cunniff, C., Nicholas, J., Reaven, J., and Rice, C.E. (2010). Autism spectrum disorder and co-occurring developmental, psychiatric, and medical conditions among children in multiple populations of the United States. J. Dev. Behav. Pediatr. *31*, 267–275.

Lin, Z. (2020). TrackMo: An Animal Tracking Toolbox for Behavioral Experiments (Github).

Martínez-Noël, G., Galligan, J.T., Sowa, M.E., Arndt, V., Overton, T.M., Harper, J.W., and Howley, P.M. (2012). Identification and proteomic analysis of distinct UBE3A/E6AP protein complexes. Mol. Cell Biol. *32*, 3095–3106.

McClain, M.B., Hasty Mills, A.M., and Murphy, L.E. (2017). Inattention and hyperactivity/impulsivity among children with attention-deficit/hyperactivity-disorder, autism spectrum disorder, and intellectual disability. Res. Dev. Disabil. *70*, 175–184. https://doi.org/10.1016/j.ridd.2017.09.009.

Moretti, P., Bouwknecht, J.A., Teague, R., Paylor, R., and Zoghbi, H.Y. (2005). Abnormalities of social interactions and home-cage behavior in a mouse model of Rett syndrome. Hum. Mol. Genet. *14*, 205–220.

Murakami, Y., Imamura, Y., Saito, K., Sakai, D., and Motoyama, J. (2019). Altered kynurenine pathway metabolites in a mouse model of human attention-deficit hyperactivity/autism spectrum disorders: a potential new biological diagnostic marker. Sci. Rep. *9*, 13182. https://doi.org/10.1038/s41598-019-49781-y.

Nadeem, A., Ahmad, S.F., Al-Harbi, N.O., AL-Ayadhi, L.Y., Al-Ayadhi, L.Y., Attia, S.M., Alasmari, A.F., As Sobeai, H.M., and Bakheet, S.A. (2020). Ubiquitous plasticizer, Di-(2-ethylhexyl) phthalate enhances existing inflammatory profile in monocytes of children with autism. Toxicology *446*, 152597. https://doi.org/10.1016/j.tox.2020.152597.

Nadeem, A., Ahmad, S.F., Al-Harbi, N.O., Attia, S.M., Bakheet, S.A., Alsanea, S., Ali, N., Albekairi, T.H., and Alsaleh, N.B. (2021). Aggravation of autism-like behavior in BTBR T+tf/J mice by environmental pollutant, di-(2-ethylhexyl) phthalate: role of nuclear factor erythroid 2-related factor 2 and oxidative enzymes in innate immune cells and cerebellum. Int. Immunopharmacol. *91*, 107323. https://doi.org/10.1016/j.intimp.2020.107323.

Nadeem, A., Ahmad, S.F., Al-Harbi, N.O., Attia, S.M., Bakheet, S.A., Ibrahim, K.E., Alqahtani, F., and Alqinyah, M. (2019). Nrf2 activator, sulforaphane ameliorates autism-like symptoms through suppression of Th17 related signaling and rectification of oxidant-antioxidant imbalance in periphery and brain of BTBR T+tf/J mice. Behav. Brain Res. *364*, 213–224. https://doi.org/10.1016/j.bbr.2019.02.031.

Nicklas, S., Hillje, A.L., Okawa, S., Rudolph, I.M., Collmann, F.M., van Wuellen, T., Del Sol, A., and Schwamborn, J.C. (2019). A complex of the ubiquitin ligase TRIM32 and the deubiquitinase USP7 balances the level of c-Myc ubiquitination and thereby determines neural stem cell fate specification. Cell Death Differ. *26*, 728–740.

Peñagarikano, O., Abrahams, B.S., Herman, E.I., Winden, K.D., Gdalyahu, A., Dong, H., Sonnenblick, L.I., Gruver, R., Almajano, J., Bragin, A., et al. (2011). Absence of CNTNAP2 leads to epilepsy, neuronal migration abnormalities, and core autism-related deficits. Cell *147*, 235–246.

Radyushkin, K., Hammerschmidt, K., Boretius, S., Varoqueaux, F., El-Kordi, A., Ronnenberg, A., Winter, D., Frahm, J., Fischer, J., Brose, N., et al. (2009). Neuroligin-3-deficient mice: model of a monogenic heritable form of autism with an olfactory deficit. Genes Brain Behav. *8*, 416–425.

Riedl, S.J., Renatus, M., Schwarzenbacher, R., Zhou, Q., Sun, C., Fesik, S.W., Liddington, R.C., and Salvesen, G.S. (2001). Structural basis for the inhibition of caspase-3 by XIAP. Cell *104*, 791–800.

Robinson, E.B., Neale, B.M., and Hyman, S.E. (2015). Genetic research in autism spectrum disorders. Curr. Opin. Pediatr. *27*, 685–691.

Sanders, S.J., Ercan-Sencicek, A.G., Hus, V., Luo, R., Murtha, M.T., Moreno-De-Luca, D., Chu, S.H., Moreau, M.P., Gupta, A.R., Thomson, S.A., et al. (2011). Multiple recurrent de novo CNVs, including duplications of the 7q11.23 Williams syndrome region, are strongly associated with autism. Neuron *70*, 863–885.

Satterstrom, F.K., Kosmicki, J.A., Wang, J., Breen, M.S., De Rubeis, S., An, J.Y., Peng, M., Collins, R., Grove, J., Klei, L., et al. (2020). Large-scale exome sequencing study implicates both developmental and functional changes in the neurobiology of autism. Cell *180*, 568–584.e23.

Schaaf, C.P., Gonzalez-Garay, M.L., Xia, F., Potocki, L., Gripp, K.W., Zhang, B., Peters, B.A., McElwain, M.A., Drmanac, R., Beaudet, A.L., et al. (2013). Truncating mutations of MAGEL2 cause Prader-Willi phenotypes and autism. Nat. Genet. *45*, 1405–1408.

Schmeisser, M.J., Ey, E., Wegener, S., Bockmann, J., Stempel, A.V., Kuebler, A., Janssen, A.L., Udvardi, P.T., Shiban, E., Spilker, C., et al. (2012). Autistic-like behaviours and hyperactivity in mice lacking ProSAP1/Shank2. Nature *486*, 256–260.

Sokolowski, J.D., Gamage, K.K., Heffron, D.S., Leblanc, A.C., Deppmann, C.D., and Mandell, J.W. (2014). Caspase-mediated cleavage of actin and tubulin is a common feature and sensitive marker of axonal degeneration in neural development and injury. Acta Neuropathol. Commun. *2*, 16. https://doi.org/10.1186/2051-5960-2-16.

Song, M.S., Salmena, L., Carracedo, A., Egia, A., Lo-Coco, F., Teruya-Feldstein, J., and Pandolfi, P.P. (2008). The deubiquitinylation and localization of PTEN are regulated by a HAUSP-PML network. Nature *455*, 813–817.

Stoppel, D.C., and Anderson, M.P. (2017). Hypersociability in the Angelman syndrome mouse model. Exp. Neurol. *293*, 137–143. https://doi.org/10.1016/j.expneurol.2017.04.002.

Sukoff Rizzo, S.J., and Crawley, J.N. (2017). Behavioral phenotyping assays for genetic mouse models of neurodevelopmental, neurodegenerative, and psychiatric disorders. Annu. Rev. Anim. Biosci. *5*, 371–389. https://doi.org/10.1146/annurev-animal-022516-022754.

Suzuki, Y., Nakabayashi, Y., and Takahashi, R. (2001a). Ubiquitin-protein ligase activity of X-linked inhibitor of apoptosis protein promotes proteasomal degradation of caspase-3 and enhances its anti-apoptotic effect in Fas-induced cell death. Proc. Natl. Acad. Sci. USA *98*, 8662–8667.

Suzuki, Y., Nakabayashi, Y., Nakata, K., Reed, J.C., and Takahashi, R. (2001b). X-linked inhibitor of apoptosis protein (XIAP) inhibits caspase-3 and -7 in distinct modes. J. Biol. Chem. *276*, 27058–27063.

Toth, M. (2019). The other side of the coin: Hypersociability. Genes Brain Behav. *18*, e12512. https://doi.org/10.1111/gbb.12512.

Tse, M.K., Hui, S.K., Yang, Y., Yin, S.T., Hu, H.Y., Zou, B., Wong, B.C.Y., and Sze, K.H. (2011).

Structural analysis of the UBA domain of X-linked inhibitor of apoptosis protein reveals different surfaces for ubiquitin-binding and self-association. PLoS One *6*, e28511. https://doi.org/10.1371/journal.pone.0028511.

Uhlen, M., Fagerberg, L., Hallstrom, B.M., Lindskog, C., Oksvold, P., Mardinoglu, A., Sivertsson, A., Kampf, C., Sjostedt, E., Asplund, A., et al. (2015). Proteomics. Tissue-based map of the human proteome. Science *347*, 1260419. https://doi.org/10.1126/science.1260419.

Unsain, N., Higgins, J.M., Parker, K.N., Johnstone, A.D., and Barker, P.A. (2013). XIAP regulates caspase activity in degenerating axons. Cell Rep. *4*, 751–763.

van der Horst, A., de Vries-Smits, A.M.M., Brenkman, A.B., van Triest, M.H., van den Broek, N., Colland, F., Maurice, M.M., and Burgering, B.M.T. (2006). FOXO4 transcriptional activity is regulated by monoubiquitination and USP7/HAUSP. Nat. Cell Biol. *8*, 1064–1073.

Vaux, D.L., and Silke, J. (2005). IAPs, RINGs and ubiquitylation. Nat. Rev. Mol. Cell Biol. *6*, 287–297.

Vogt, D., Cho, K.K.A., Lee, A.T., Sohal, V.S., and Rubenstein, J.L.R. (2015). The parvalbumin/somatostatin ratio is increased in Pten mutant mice and by human PTEN ASD alleles. Cell Rep. *11*, 944–956.

Wang, L., Almeida, L.E., Nettleton, M., Khaibullina, A., Albani, S., Kamimura, S., Nouraie, M., and Quezado, Z.M. (2016). Altered nocifensive behavior in animal models of autism spectrum disorder: the role of the nicotinic cholinergic system. Neuropharmacology *111*, 323–334. https://doi.org/10.1016/j.neuropharm.2016.09.013.

Yang, Y., Fang, S., Jensen, J.P., Weissman, A.M., and Ashwell, J.D. (2000). Ubiquitin protein ligase activity of IAPs and their degradation in proteasomes in response to apoptotic stimuli. Science *288*, 874–877.

Zheng, F., Kasper, L.H., Bedford, D.C., Lerach, S., Teubner, B.J.W., and Brindle, P.K. (2016). Mutation of the CH1 domain in the histone acetyltransferase CREBBP results in autism-relevant behaviors in mice. PLoS One *11*, e0146366. https://doi.org/10.1371/journal.pone.0146366.

Zhu, Q., Sharma, N., He, J., Wani, G., and Wani, A.A. (2015). USP7 deubiquitinase promotes ubiquitin-dependent DNA damage signaling by stabilizing RNF168. Cell Cycle *14*, 1413–1425.

STAR★METHODS

KEY RESOURCES TABLE

REAGENT or RESOURCE	SOURCE	IDENTIFIER
Antibodies		
mouse anti-USP7	Santa Cruz	Cat# sc-137008; RRID: AB_2214163
rabbit anti-XIAP	Bioss Antibodies	Cat# bs-1281r; RRID: AB_10856518
rabbit anti-XIAP	Sigma-Aldrich	Cat# PRS3331; RRID: AB_1858883
mouse anti-FLAG tag DYKDDDDK	Cell Signaling Technology	Cat# 8146; RRID: AB_10950495
mouse anti-PSD95	synaptic systems	Cat# 124011; RRID: AB_10804286
mouse anti-E6AP	Sigma-Aldrich	Cat# E8655; RRID: AB_261956
rabbit anti-cleaved caspase-3	Cell Signaling Technology	Cat# 9661; RRID: AB_2341188
anti-GAPDH	EMD Millipore	Cat# MAB374; RRID: AB_2107445
mouse anti-α tubulin	Sigma-Aldrich	Cat# T9026; RRID: AB_477593
rabbit anti-cleaved tubulin (TubΔCasp6)	provided kindly by Andrea LeBlanc at McGill University	N/A
mouse anti-NeuN	EMD Millipore	Cat# MAB377; RRID: AB_2298772
rabbit anti-Ubiquitin	Abcam	Cat# ab19247; RRID: AB_444805
mouse-IgG-HRP	Bio-Rad	Cat# 170-6516; RRID: AB_11125547
Rabbit-IgG-HRP	Bio-Rad	Cat# 170-6515; RRID: AB_11125142
mouse Alexa Fluor 488	Invitrogen	Cat# A21121; RRID: AB_2535764
rabbit Alexa Fluor 488	Invitrogen	Cat# A11094; RRID: AB_221544
mouse Alexa Fluor 555	Invitrogen	Cat# A21127; RRID: AB_141596
rabbit Alexa Fluor 555	Invitrogen	Cat# A21428; RRID: AB_2535849
Bacterial and virus strains		
AAV2 system (transfected adenovirus helper (XX680) and AAV2 helper (pXR2))	provided kindly by Angela Ho lab at Boston University	N/A
AAV-ReaChR-citrine	Addgene	RRID: Addgene_50954
Chemicals, peptides, and recombinant proteins		
HBX41108	Tocris	Cat# 4285
MG132	Sigma-Aldrich	Cat# 7449
Polyethylenimine	Polysciences	Cat# 23,966
Lipofectamine 2000	Invitrogen	Cat# 11668019
fast green dye	Sigma-Aldrich	Cat# F7258
Experimental models: Cell lines		
Human embryonic kidney (HEK) 293T cells	N/A	N/A
Experimental models: Organisms/strains		
FVB/NJ WT mouse	THE JACKSON LABORATORY	RRID: IMSR_JAX:001800
CD-1 mouse	Charles River Laboratories	RRID: IMSR_CRL:022
Sprague–Dawley rat	Charles River Laboratories	N/A
Oligonucleotides		
siRNA target sequence: USP7 #1: 5′-GAAGGUACUUUAAGAGAUC-3′	Thermofisher	N/A

(*Continued on next page*)

Continued

REAGENT or RESOURCE	SOURCE	IDENTIFIER
siRNA target sequence: USP7 #2: 5′-ACCCUUGGACAAUAUUCCU-3	Thermofisher	N/A
siRNA target sequence: USP7 #3: 5′-CUAAGGACCCUGCAAAUUA-3′	Thermofisher	N/A
Primer USP7: TAAGCAGAATTC ATGAACCACCAGCAGCAG	Thermofisher	N/A
siRNA target sequence: XIAP #1: 5′-CTGGACAGGTTGTAGATAT-3′	Thermofisher	N/A
siRNA target sequence: XIAP #2: 5′-TTGCAGATTTATCAATGGT-3′	Thermofisher	N/A
siRNA target sequence: XIAP #3: 5′-GTGAATGAGTCACCTGCAT-3′	Thermofisher	N/A
Recombinant DNA		
pCI-neo Flag HAUSP	Addgene	RRID: Addgene_16655
pEBB-XIAP	Addgene	RRID: Addgene_11558
p4054-E6AP	Addgene	RRID: Addgene_8658
AAV-ReaChR-citrine	Addgene	RRID: Addgene_50954
pLKO.3G	Addgene	RRID: Addgene_14748
pCGLH GFP	provided kindly by Angela Ho lab at Boston University	N/A
pCGLH RFP	This paper	N/A
Software and algorithms		
ImageJ	N/A	https://wsr.imagej.net/distros/win/ij153-win-java8.zip
TrackMo	https://github.com/zudi-lin/tracking_toolbox	N/A
Prism 8.0	GraphPad Software	N/A

RESOURCE AVAILABILITY

Lead contact

Further information and requests for resources and reagents should be directed to and will be fulfilled by the lead contact, Heng-Ye Man (hman@bu.edu).

Materials availability

To make AAV USP7, USP7 was subcloned into AAV-ReaChR-citrine (Addgene, #50954) using the BamHI and HindIII restriction sites. For *in utero* electroporation, USP7 was subcloned into the pCGLH GFP vector using BglII and SalI sites. pCGLH RFP was used as the control. For shRNAs, four USP7 shRNA sequences and three XIAP shRNA sequences were designed using BLOCK-iT^{TM} RNAi Designer (ThermoFisher Scientific) and cloned into the pLKO.3G cloning vector (Addgene; cat. # 14748) using PacI and EcoRI sites.

All those plasmids generated in this study have been deposited in DNA library in Man's lab at Boston University.

Data and code availability

- All siRNA and primer sequences are reported in KRT. Original biochemical and immunostaining data reported in this paper will be shared by the lead contact upon request.
- This paper does not report original code.
- Any additional information required to reanalyze the data reported in this paper is available from the lead contact upon request.

EXPERIMENTAL MODEL AND SUBJECT DETAILS

All procedures for animal study were conducted in accordance with the National Institutes of Health Guide for the Care and Use of Laboratory Animals and were approved by the Institutional Animal Care and Use Committee at Boston University.

FVB/NJ WT mouse (001800 - FVB Strain Details (jax.org)) pups (11 males and 11 females) on postnatal day 0 were used for Bilateral intracerebroventricular (ICV) injection; pregnant CD-1 dams at embryonic day 14.5 (CD-1® IGS Mouse | Charles River (criver.com))) were used for *in utero* electroporation (IUE).

Primary cultured hippocampal neurons were prepared from E18 rat embryos (Huo et al., 2015). Sprague–Dawley rats were purchased from Charles River Laboratories Inc., Wilmington, MA, USA. Embryonic brain regions were dissected and digested with papain (0.5 mg/mL in Hanks balanced salt solution, Sigma-Aldrich; cat. # 4762) at 37°C for 15 min, then gently triturated in trituration buffer [0.1% DNase (cat. # PA5-22017 RRID: AB_11153259), 1% ovomucoid (Sigma-Aldrich; cat. # T2011)/1% bovine serum albumin (Sigma-Aldrich; cat. #05470) in Dulbecco's modified Eagle's medium] until neurons were fully dissociated. Dissociated neurons were seeded onto poly-L-lysine-coated coverslips (Carolina, Burlington, NC; cat. # 633013). Neurons were maintained in Neurobasal medium (Gibco, Rockville, MD, USA) supplemented with 2% B27, 1% horse serum, 1% penicillin/streptomycin, and 1% L-glutamine for 2 weeks until use. One week after plating, *5-fluorodeoxyuridine* (5 μM) was added to the media to inhibit glial growth. All cells were maintained in a humidified incubator containing 5% CO_2.

Human embryonic kidney (HEK) 293T cells were cultured in Dulbecco's Modified Eagle Medium (Gibco) supplemented with 10% heat-inactivated fetal bovine serum and 1% penicillin/streptomycin and passaged at 90% confluency twice a week.

METHOD DETAILS

Neuronal and cell line transfection

Neuron transfections were performed with Lipofectamine 2000 (Invitrogen, Carlsbad, CA, USA) according to the manufacturer's instructions. In a 12-well culture plate, for transfection of cells per well containing 0.5 mL plating medium, 1 μL Lipofectamine 2000 and 1 μg plasmid DNA were first separately diluted in 50 μL minimal essential medium then mixed and incubated at room temperature for 20 min to form the transfection complex. The transfection complex was added to the wells and incubated at 37°C for 4 h before the medium was removed and replaced with feeding medium. Three days following the transfection of neurons, cells were fixed and immunostained or lysed for biochemical analysis. HEK 293T cells transfections were performed at approximately 70% confluency using polyethylenimine reagent (Polysciences, Warrington, PA; cat. # 23966). Two days following the transfection of HEK cells, cells were fixed and immunostained or lysed for biochemical analysis.

Viral constructs preparation and virus infection

Full length USP7 fragment from pCI-neo Flag HAUSP/USP7 (addgene, #16655) were inserted into the AAV-ReaChR-citrine vector. To package AAV particles, HEK293T cells at 60–70% confluency in 15-cm culture plates were transfected with pAAV-USP7, together with adenovirus helper plasmid (XX680) and a 10-fold excess of pXR2 containing AAV2 Rep and Cap using Polyethylenimine (Invitrogen) in OPTI-MEM (Gibco). Approximately 72 h post-transfection, cell culture medium and cell debris were collected separately. The medium was filtered with 0.45 μm filter. Cell debris were collected with 2 mL Tris-HCl and frozen (−70°C) and thawed (37°C) repeatedly for eight times, followed by centrifugation for 30 min at the speed of 3000 rpm, 4°C. The supernatant was mixed with filtered medium collected earlier, and PEG-it (1:5) was added and kept at 4°C overnight. Following centrifugation (1500 rpm, 45 min, 4°C) the pellet was resuspended with 100 μL cold PBS. Aliquots of the virus were stored in a −80°C freezer for future use.

Biochemical analysis of protein ubiquitination

Cultured cortical neurons or HEK cells were rinsed with cold aCSF and collected in 200 μL lysis buffer [50 mM Tris-HCl pH 7.4, 150 mM NaCl, 1% NP40, 1% Sodium deoxycholate (SDOC) and 1% sodium dodecyl sulfate (SDS)] containing mini cOmplete protease inhibitors (Hoffmann-La Roche Grenzacherstrasse, Basel, Switzerland). The high SDS concentration was applied to avoid conventional protein–protein interaction. Lysates were further solubilized by sonication and 10 min incubation on ice followed by centrifugation

for 10 min at 13 000 g. Supernatant was adjusted to 500 μL with lysis buffer and incubated 3 h on rotation at 4°C with 1μL antibodies against XIAP and protein A-Sepharose beads (Santa Cruz Biotechnology, Santa Cruz, CA, USA). Immunocomplexes were washed three times with ice-cold lysis buffer without SDS (50 mM Tris-HCl pH 7.4, 150 mM NaCl, 1% NP40, 1% SDOC), resuspended in 2X Laemmli buffer and denatured at 95°C for 10 min.

Western blot

Primary neurons cultured in six-well plates (10^6 cells/well) were treated with virus at the time of plating day. Neurons were lysed in Laemmli 2× sample buffer (4% SDS, 10% 2-mercaptoethanol, 20% glycerol, 0.004% bromophenol blue, and 0.125 M Tris-HCl) and boiled for 10 min at 95°C for SDS-PAGE electrophoresis. After separation in SDS-PAGE, proteins were transferred to polyvinylidene fluoride membranes (Bio-Rad, Richmond, CA) and probed for different targets with the stated antibodies (in Key resources table). The concentration of primary antibody is 1:1000, and the secondary antibody is 1:5000. Immunoblots were visualized using a chemiluminescence detection system (Sapphire Biomolecular Imager, Azure biosystems, CA, USA), and analyzed using ImageJ.

In utero electroporation

In utero electroporation (IUE) was performed on timed pregnant CD-1 dams at embryonic day 14.5 (Gilbert and Man, 2016). Dams were anesthetized via i.p. injection of a ketamine/xylazine mixture. The fur over the abdomen was shaved and cleaned with 70% ethanol. An incision (2.5 cm) in the abdominal cavity was made to expose the uterine horns. 1–2 μL of plasmid DNA mixed with 0.1% fast green dye (Sigma-Aldrich; cat. #F7258) was injected into the ventricle through the uterine wall and amniotic sac using a pulled-glass micropipette. The plasmid vectors were used at a final concentration of 2–3 μg/μL. The anode of a Tweezertrode (Harvard Apparatus, Holliston, MA) was placed over the dorsal telencephalon above the uterine muscle, and four 35 V pulses (50 ms duration separated by a 950 ms interval) were delivered from a BTX ECM830 pulse generator (Harvard Apparatus). The gap between the electrodes was filled with warm saline before electric pulses. After electroporation, the uterine horns were returned to the abdomen, and the cavity was filled with a warm saline solution. The surgical incisions were closed with sutures. The dams were then placed in a clean cage and monitored closely during recovery (about 2 hours). The pups were allowed to mature with the mother until the time as indicated.

Intraventricular brain injection of adeno-associated virus (AAV2) in neonatal mice

Bilateral intracerebroventricular (ICV) injections were performed in FVB/NJ WT mouse (https://www.jax.org/strain/001800) pups on postnatal day 0 (P0). Briefly, Newborn FVB mice were cryoanesthetized and subsequently placed on a cold metal plate. The injection system consisted of a 30 gauge needle, 20 cm PE20 plastic tube, 5 μL Hamilton syringe and a pump (KD Scientific Model 100 series). A needle was used to pierce the skull at the site that is approximately two-fifth of the distance between the lamda and eye, and 2 μL of AAV was injected into each cerebral ventricle at the speed of 0.2 μL/min. Neonatal mice were kept with their parents until weaned. Mice were sacrificed at P55 post-injection. All mice were behaviorally assessed before being euthanized for biochemical and histological analysis.

Behavioral tests

Behavioral tests were performed on mice from the age of P30 to P55. The sequential order and the specific times of behavioral tests are: Habituation (P31-33), Open field test (P34), Homecage behavior test (P35-36), Hot plate test (P37-39), Marble bury test (P41-42), Novel object recognition (P44-48), and Three-chamber test (P50-54).

Open field test

Mice were habituated to the testing room over 3 d and handled for 5 min each day. Lights in the testing room were off except for a small desk lamp in the corner allowing the experimenter to see. On the test day, each mouse was singly placed into the center of an open-field arena (40 × 40 × 30 cm^3), and allowed to freely explore the chamber. Video recordings were captured with a Logitech c920 webcam during the test. Track length was analyzed using TrackMo (https://github.com/zudi-lin/tracking_toolbox, 2020) (Lin, 2020). The chamber was cleaned with 70% ethanol thoroughly after the test.

Homecage behavior test

Mice were single-housed and tested in their home cage. Video recordings were captured with a Logitech c920 webcam for 30 min, and the final 5 min recordings were used to quantify the grooming, rearing, digging, climbing, circling and jumping behaviors. A 1 s refractory period was introduced to avoid counting high frequency repetitive behavior such as grooming and digging (Moretti et al., 2005).

Hot plate test

Pain sensitivity of mice was evaluated through the hot plate test (Wang et al., 2016). The temperature of the hot plate was set to 55°C. Mice were placed on the surface of the hot plate and covered by a glass transparent cylinder, 25 cm high and 12 cm diameter. The latency to response was measured when the hind paw lick or jump occurred. Prior to the test, a two-day habituation session (15 min/day) was given to let mice habituate the surface of the non-heated hot plate and the covered cylinder before the test.

Marble burying test

Marble burying was conducted in the animal's home cage with a 3-inch-thick layer of fresh pine chip bedding. Sixteen shiny glass marbles (0.25-inch diameter) were arranged in a 4 × 4 grid on top of the bedding (Gilbert et al., 2020). Mice were singly placed back into the cage and allowed to move freely and bury marbles. Video recordings were captured with a Logitech c920 webcam during the test and the number of marbles buried after 5, 10, 15, 25 and 30 min was quantified.

Novel object recognition (NOR) test

The NOR protocol consists of habituation, training, and test sessions (Leger et al., 2013). Habituation: mice were exposed to an open-field apparatus twice a day for three days before the test (10 min for each session). Training: two identical objects (falcon tissue culture flask filled with beddings) were placed in two corners of the arena and animals were allowed to explore for 10 min on day 4. Testing: one object was replaced by a new one (tower of Lego bricks) for this session. Video recordings were captured for 5 min, and track length was quantified. Recorded videos were analyzed by TrackMo and the discrimination index (DI) was calculated by dividing the exploration time of the novel object by the total exploration time.

Three-chamber test

A three-chambered box was constructed from a 0.75-inch-thick white plastic board measuring 65 × 28 × 28 cm. The walls to the center chamber had 10 × 10 cm cut-out doors allowing movement between chambers. The two side chambers contained small wire cages to house social mice. Habituation: Before the test, mice were habituated to the apparatus with empty wire cages, over a three-day period for 10 min each session, and allowed to move freely among all three chambers. Social preference session: On the testing day, mice were singly placed into the center, with the doors blocked with plastic boards, and a social mouse (Mouse 1) was placed into the left-side wire cage. The doors were unblocked, and the test mouse was allowed to move freely within the apparatus for 5 min. Social novelty session: During this session, the test mouse was returned to the center chamber, and the doors were blocked again. A second mouse (Novel Mouse) was placed into the right chamber under the wire cage. The center doors were unblocked, and the test mouse was allowed to move freely within the apparatus for another 5 min. The entire apparatus was wiped with 70% ethanol between mice to eliminate odor cues between animals. Video recordings were captured with a Logitech c920 webcam during the test. The time spent interacting with each mouse or empty cage (nose $\leq$2 cm), the time spent in each chamber, and the locomotion tracks were scored using TrackMo (Lin, 2020). The preference index (PI) was calculated by dividing the time spend in the Mouse 1 chamber by the total time spend in both Mouse 1 and Empty (or Novel Mouse) chambers.

Immunohistochemistry of brain slices

To collect the electroporated brains, mice older than P0 were anesthetized with an i.p. injection of ketamine/xylazine and transcardially perfused with warmed PBS and fix solution (4% paraformaldehyde in PBS). Brains were removed and placed into fixation solution at 4°C for 4–6 h, followed by a 2-3-day incubation in a 30% sucrose PBS solution at 4°C. Brains were then frozen in OCT (Tissue-Tek; cat. # 25608-930) and cut into 25-μm sections using Leica CM 1850 cryostat (Leica Biosystems, Buffalo Grove, IL) at −20°C. For P0 animals, brains were kept intact in the skull for fixation and slicing.

Sections were mounted onto SuperFrost microscope slides (Fisher Scientific) and stored at −80°C for future use. Before immunostaining, sections were rinsed with PBS for a minimum of 2 h and antigen retrieval was performed by microwaving brain sections in sodium citrate buffer (10 mm, pH 6) at 800 W for 1 min followed by 80 W for 10 min. Sections were then blocked in a 5% goat serum plus 0.3% Triton X-100/PBS solution for 1 h followed by incubation with primary antibodies overnight at 4°C. The following day, sections were washed with PBS and incubated with the appropriate Alexa Fluor-conjugated secondary antibodies. Sections were then mounted with ProLong-Gold mounting medium (Invitrogen), allowed to dry at room temperature overnight, and stored at −20°C.

QUANTIFICATION AND STATISTICAL ANALYSIS

Experimental design and statistical analyses

For the *in vitro* experiments, each experiment was repeated at least three times. For all structure analysis and immunostaining results, n represents neurons from three to four individual experiments. For western blot results, n refers to experimental replicates. The IUE experiment was performed twice, and in each batch, there were 2-3 pups per group (Control and USP7 group). For the virus injection and behavioral experiments, three batches of pups were used (9 for control and 13 for USP7 in total). The behavior tests were performed and analyzed with the experimenter blinded to the identity of the animals.

Repeated measures ANOVA was used for the sholl analysis, the CHX degradation experiment *in vitro*, and the marble burying test. One-way ANOVA with post hoc Tukey's test or Tamhane's test was used for all experiments that had more than two groups. An unpaired Student's *t* test was used for the other two-group analyses.

Prism 8.0 (GraphPad Software) was used for the graphics and statistical analyses; $p < 0.05$ was considered statistically significant. Data are presented as mean ± SEM.

Sholl analysis

Dendrites were traced from images of neurons stained with MAP2 using the NeuronJ (RRID: SCR_002074) plugin in ImageJ (RRID: SCR_003070). The Snapshot tool in NeuronJ was used to save the tracings as an image file that was converted to 8-bit, and these images were analyzed with the Sholl analysis plugin in ImageJ. The range of measurement was set using the straight-line tool traced from the center of the soma to the outermost neurite. Dendrite intersections were analyzed from a starting radius of 10 μm with 10 μm steps to the outer radius. The resulting numbers of intersections per cell were used to calculate the mean and SEM for each radius interval.